Flow Regimes, SST Forcing, and Climate Noise: Results from Large GCM Ensembles

David M. Straus
George Mason University
Center for Ocean-Land-Atmosphere Studies

Franco Molteni
International Centre for Theoretical Physics

Corresponding author address:
David Straus
4041 Powder Mill Rd., Suite 302
Calverton, MD 20705

email: straus@cola.iges.org
January 16, 2003

Abstract.

A flow regime analysis has been applied to 55-member ensembles of seasonal simulations of the Center for Ocean-Land-Atmosphere Studies (COLA) general circulation model (GCM) for each of 18 winters. The members of each ensemble utilize the same prescribed, observed weekly varying sea surface temperature (SST).

The distinction is made between intra-seasonal fluctuations containing periods of 10 days to a season (low frequency) and the ultra-low frequency fluctuations. The latter are expressed in terms of a second-order polynomial fitted to each seasonal time series by a least-squares expansion. The GCM low-frequency variance of 200 hPa height is comparable to that from reanalyses in the Pacific North-American region. The intra-ensemble variability contributes as much as the low frequency variance to the total GCM variance. The low frequency variance of the GCM integrated over the North Pacific ($160^oE - 110^o$,$40^o - 80^o$) is highly correlated with the Niño-3 and Niño-3.4 indices (-0.79 and -0.75, respectively); the correlations for reanalysis are -0.65 and -0.61. The total GCM variance correlations with the two indices are -0.84 and -0.80

The partitioning algorithm of Michelangeli et al. (1995) was applied to each ensemble separately. Only the mean seasonal cycle (ensemble mean ultra-low frequency component) was removed from each ensemble; the intra-ensemble variability of ultra-low frequency components, including the seasonal mean, is retained. Both 200 hPa heights and zonal winds in the Pacific-North American sector ($150^oE - 30^oW$, $20^oN - 80^oN$) were considered.

The data were truncated to include the 4 leading empirical orthogonal functions (EOFs). The most probable cluster number (k) was chosen to range from 2 to 6. The ratio of the variance between cluster centroids (averages) to the intra-cluster variance, taken over all winters, is negatively correlated (value of about -0.8 or less) with the Niño3 and Niño3.4 indices of sea surface temperature (SST) for all values of k. The variance ratio is negatively correlated (coefficient of -0.8 or smaller) with the projection of the ensemble seasonal mean on the leading EOF of all 18 ensemble seasonal means (SST signal pattern).

Significance vis-a-vis a corresponding red-noise model for each number of clusters (k) was assessed. The winters of 1982/83, 1986/87 and 1997/98 (all El Niño years) failed to show significant clustering for all k from 2 to 6. All other winters were significant for a range of k. The forcing from warm El Niño - Southern Oscillation (ENSO) events tends to suppress the regime behavior occurring in near-normal and cold ENSO winters.

The clustering during the remaining 15 winters showed is of reproducible (for all k) as measured by the average anomaly correlation between cluster centroids of 100 half-length samples. Dynamical consistency between clusters of the 200 hPa zonal wind field and height field was established.

The range of cluster number k passing all significance, reproducibility and dynamical consistency tests ranged from k=2 to k=6 depending on winter. For all significant k, one of the clusters corresponds to a pattern showing a strong amplified ridge over the Gulf of Alaska, a trough extending from the southwest to the northeast across central North America, and a weaker ridge over Florida. The same pattern is a dominant pattern in the intra-ensemble variability of seasonal means, or climate noise, as seen by the leading EOF of climate noise

for all 18 years.

The clustering algorithm was repeated using only the low frequency fluctuations of 200 hPa height, thus excluding all ultra-low frequency intra-ensemble variability. The resulting patterns are virtually identical to those of the preceding calculation, although the anomalies of the cluster means are somewhat weaker, and the significance levels reduced.

1. Introduction

Recent efforts to better quantify the predictability of seasonal climate have underscored the importance of intra-seasonal low frequency variability from several points of view. Clearly low frequency fluctuations strongly affect the extremes of weather, which are themselves important elements of seasonal climate, because they define the background state on which the synoptic disturbances propagate. But the important point from the view of seasonal predictability is that their statistical properties are dependent on the boundary forcing. This has been noted specifically in relationship to the El Niño Southern Oscillation (ENSO) phenomenon (Chen and van den Dool, 1997; Trenberth and Hurrell, 1994; Molteni and Corti, 1998; Shukla et al., 2000; Straus and Shukla, 1997). This means that potential seasonal predictability based on knowledge of the underlying tropical SST, often thought of in terms of the seasonal mean, can be extended to encompass the likelihood of shifts in both the low frequency component of the circulation and the associated storm tracks (Compo et al., 2001).

However, chaotic systems have the property that even their long-term mean may be unpredictable (Lorenz, 1964). This realization led to the understanding that the potential predictability of the seasonal mean itself is limited by the chaotic nature of atmospheric dynamics, particularly in mid-latitudes (Shukla et al., 2000). The uncertainty in, for example, the seasonal mean anomaly associated with El Niño events can be only roughly estimated from observations (since each El Niño event is unique, see Kumar and Hoerling 1997). Ensemble integrations of GCMs, on the other hand, provide an approach to estimating both

the predictable component (signal) and un-predictable component (noise) of the seasonal mean (Branković and Palmer, 2000; Graham et al., 2000; Chang et al., 2000; Kumar et al., 2000; Sardeshmukh et al., 2000; Shukla et al., 2000; Straus and Shukla, 2000; Schubert et al., 2001; Straus and Shukla, 2002).

The understanding that SST-forced predictability must be thought of in terms of the probability distribution of all elements of the seasonal climate, including the seasonal mean, low frequency fluctuations and storm track changes, has led to some explicit model-based attempts to estimate aspects of these distributions. Straus and Shukla 2002 use modest ensembles (9 members) for 30 winters (with observed SSTs) and show the change in the unpredictable component of the seasonal mean ("climate noise") with ENSO state. Compo et al. (2001) use very large ensembles (180 members) for one El Niño and one La Niña year, and show maps of the El Niño-Southern Oscillation (ENSO) related shifts in the variances on synoptic, low frequency, monthly and seasonal mean time scales. Sardeshmukh et al. (2000) point out that such large ensembles are critical for obtaining reliable estimates of the changes in probability distribution.

While maps of the ENSO related change of variance are critical for point by point predictability estimates, no information about preferred spatial patterns is provided. Yet it has been established that a few important regional and hemispheric patterns do dominate the wintertime low-frequency variability in both nature and in models, and it has been possible to substantiate this using multiple methodologies of cluster analysis (Corti et al., 1999; Cheng and Wallace, 1993; Kimoto and Ghil, 1993a,b; Michelangeli et al., 1995; Haines and

Hannachi, 1995) While the cluster techniques do not yield completely unambiguous results (especially for observations, where the sample size is quite limited), general agreement among a number of approaches, particularly in the Pacific region, has been encouraging.

The purpose of this article is to analyze the preferred structures (weather regimes) of the circulation in the Pacific region on time scales longer than 10 days, and in particular to study their dependence on the ENSO SST state. For this purpose we apply cluster analysis to large (55-member) seasonal ensemble simulations of a GCM for 18 recent winters. (Each ensemble uses the same observed weekly SST evolution.) The variability of interest includes not only the variability of the seasonal means (seasonal mean climate noise) and the traditional low frequency intra-seasonal variance, but also the intra-seasonal variance arising from anomalous fluctuations with periods longer than a season (ultra-low frequency). The latter contributes to, for example, the variability of monthly means for the single year ensembles of Compo. The results will show explicitly for the first time that the regime structures characterizing low and ultra-low frequency variance are related to the chaotic variability of seasonal means.

Relatively little previous work has been done to explore the relationship between regime behavior and external SST forcing. Toth (1991, 1993b) examined quasi-stationary states in the Northern Hemisphere 700 hPa height field and found a number of significant clusters, some of which were associated with warm tropical Pacific SST anomalies. On the other hand, the works of Kimoto (1989) and Molteni and Corti (1998) suggest that regime behavior is more likely to be associated with cold Pacific SSTs. The relationship of our findings from GCM simulations to this previous work will be discussed further on in the paper.

It is important to state at the outset that the analysis of each 55-member ensemble of simulations is carried out completely separately. The analysis of one winter is done in isolation from the results of any other winter. (The only exception to this is that the weather regimes themselves will be presented in terms of anomalies from the total model climate.) This means that the most obvious effect of SST forcing, namely to change the expected mean state, is not explicitly considered; only the indirect effects are. The analysis to be presented could be adapted to the true forecast mode, where of course the SST would have to be predicted first.

In section 2 we will discuss the general circulation model experiments, and the model data used. Section 3 presents the methods of analysis of time scales, and the dependence of the variance on tropical Pacific SST indices. A brief review of clustering methodologies is presented in Section 4, along with a more detailed description of the method used here to identify the preferred regimes, and the associated significance, reproducibility, and dynamical consistency tests. The regimes obtained for individual winters are described in Section 5. Section 6 presents a cluster analysis of the model data after removing the climate noise and the ultra-low frequency intra-seasonal variations, so that the remaining fluctuations have periods of 10-96 days. Section 7 presents a summary, discussion and conclusions.

2. GCM Data and Data Reduction

(a) COLA GCM and SST data. This GCM is Version 2.2 of the COLA GCM, run at horizontal spectral resolution of triangular T63, with 18 sigma levels. It uses the dynamical core of the National Center for Atmospheric Research Center Community Model version 3

(CCM3) described in Kiehl et al. (1998); otherwise it is as described in Schneider (2002). The dependent variables of the model are spectrally treated, except the moisture variable, which is advected using the semi-Lagrangian technique. The land surface model (LSM), which is coupled to the atmospheric model, is the Simplified Biosphere Model (SSiB) documented in Xue et al. (1991). The parameterization of deep convection is the relaxed Arakawa- Schubert scheme (Moorthi and Suarez, 1992). For further details consult Schneider (2002).

There are 55 members in each ensemble. Initial conditions (ICs) 1-5 are obtained from the NCEP reanalyses for 00 UTC on the last five days of November. Initial conditions 6-10 were obtained from ICs 1-5 by adding a perturbation which consists of the the difference between the analyses 12 hours after and 12 hours before. The remaining 45 ICs were obtained by adding 9 further perturbations to ICs 1-5. These perturbations were chosenly randomly from a larger set of perturbations consisting of 24, 48 and 72 hour differences of 06, 12 and 18 UTC NCEP reanalysis states. In each case, the two reanalysis states used to form the perturbation bracket the original IC.

The SST fields used as boundary conditions for the GCM simulations are from Reynolds (see Reynolds and Smith 1994); the data are used on a weekly basis. The Reynolds SST data set was used to create seasonal (Dec.-Mar. averaged) values of the Niño3 and Niño3.4 indices. The Niño3 (Niño3.4) index is defined as the areal average SST for the area $150^o - 90^oW$, $5^oS - 5^oN$ ($170^o - 120^oW$, $5^oS - 5^oN$).

(b) Data Reduction. The ultra-low frequency components of the GCM data are calculated from the 110 day segment (12 December - 31 March) using the Legendre decomposition of

Straus (1983), as described in Section 3. The ensemble mean of the ultra-low frequency components gives the estimate of the seasonal cycle consistent with the SST forcing for that winter. After removing only the SST-dependent seasonal cycle, the remaining daily data for 200 hPa height and wind fields are filtered with a 15-point Lanczos filter (Duchon, 1979) to remove periods shorter than about 10 days. These data then consist of 96 day time series extending from 19 December - 24 March. These time series are used in the variance calculations shown in Section 3. All 55 of these time series for each winter were used to compute EOFs and PCs, and the leading 4 EOFs (PCs) were retained in the cluster analyses. About 70% of the variance is typically explained with this truncation.

3. SST Dependence of Variance

(a). Analysis of time scales. For each calendar winter, the ensemble GCM daily data are available once per day for the 110 day period starting on 00UTC December 12. We decompose each 110-day time series at each grid point into Legendre polynomials in time, following Straus (1983). The first three components of the Legendre expansion (Straus, 1983) are just the seasonal mean, the trend, and a parabolic part; these components have time scales of longer than 110 days. Thus if $X(t)$ is the time series of any model variable at a grid point,

$$X(t) = \sum_{i=1}^{i=3} C_i \, P_i(t) + R(t), \tag{1}$$

where the C_i are coefficients and the $P_i(t)$ the Legendre time functions. The remaining components $R(t)$ contain fluctuations whose time scales are shorter than 110 days[1] The

[1]In traditional Fourier analysis, removing some estimate of the component of the time series with time

daily time series $R(T)$ is filtered in time using a 15-point digital Lanczos filter (Duchon, 1979) into a low-frequency and a high frequency component, each of length 96 days. Writing the sum of the first three components for any variable X as X_U, and the low and high frequency components of R as X_L and X_H respectively, the time series X is written as:

$$X = X_U + R = X_U + X_L + X_H \tag{2}$$

This decomposition is carried out for each ensemble member for a given winter. The average of X_U over the ensemble gives our estimate of the winter segment of the seasonal cycle consistent with the given SST evolution. Note that we do not subtract an overall climatology; this would introduce the large effects of shifts in the mean due to SST forcing which we wish to neglect in this specific study. Subtracting the ensemble mean (denoted by angular brackets), we obtain:

$$X - \langle X_U \rangle = X_U - \langle X_U \rangle + X_L + X_H = Y + X_H, \tag{3}$$

where the time series Y

$$Y = X_U - \langle X_U \rangle + X_L \tag{4}$$

contains both the deviations of the ultra-low frequency about the ensemble mean and the low frequency components. The time series Y is what we analyze in this paper. Note that

$$Y(t) - X_L(t) = X_U - \langle X_U \rangle = \sum_{i=1}^{i=3} (C_i - \langle C_i \rangle)\ P_i(t) \tag{5}$$

scales longer than the record length is necessary before fitting the time series to Fourier components in order to reduce signficant leakage.

contains both the seasonal mean climate noise ($i = 1$) and the remaining unpredictable part of the ultra-low frequency variability ($i = 2, 3$). It represents a generalized climate noise.

(b) Low Frequency Variance. Here we present observed and simulated maps of the temporal variance of the time series X_L for 200 hPa height, averaged over ensemble member (for the model) and all years. Figure 1b shows the map of the observed variance averaged over the 18 winters of 1981/82 - 1998/99 over the region of interest, $150^oE - 30^oW$, $20^oN - 80^oN$. Observed daily data for the period 12 Dec. - 31 Mar. were taken from the reanalysis of the National Centers for Environmental Prediction (Kalnay and coauthors, 1996) and were decomposed using the same filters applied to the model data.

Two centers are seen over Northern Alaska and Hudson Bay. The strength of the Alaska center is fairly strongly related to tropical Pacific SSTs, as shown by Figure 1a which presents time series of the area-integrated variance over the North Pacific region $160^oE - 210^oW, 40^oN - 80^oN$ (solid line) as well as the seasonal (Dec.-Feb. mean) values of the Niño-3 and Niño-3.4 indices (dotted and dashed lines). The correlations of the variance with the two indices are -0.65 and -0.61, respectively (see Table 1). During La Niña years the variance is enhanced, as expected from Chen and van den Dool (1997).

The GCM low frequency variance (averaged over all ensemble members and all winters) shows a very strong (and slightly shifted) center over Alaska, with 15 percent more variance than observed (Figure 2b). The simulated variance over Hudson Bay is too small, so the distinct maximum in observations becomes a shoulder here. The strength of the Pacific maximum is again strongly anti-correlated with Niño-3 and Niño-3.4, and the strength of

the correlation is somewhat higher (-0.79 and -0.75, respectively, Table 1).

The map of the temporal variance of Y, which includes the low frequency and the deviations of the ultra-low frequency about the ensemble mean, is shown in Figure 3b. It is similar in shape the low-frequency variance, but is 50 percent stronger in magnitude. Half of this increase is due to the seasonal-mean climate noise ($i = 1$ component in equation 5), and half to the remaining unpredictable part of the ultra-low frequency variability ($i = 2, 3$ in equation 5).

Interestingly, the magnitude of the correlation of the total variance with Niño-3 and Niño-3.4 (-0.84 and -0.80, respectively) is higher than the corresponding correlations with the low frequency variance only (see Table 1).

4. Cluster Analysis.

(a) Introduction. Cluster analysis is a class of objective methods that has been used extensively to obtain preferred flow regimes. These include: (1) hierarchical methods (Cheng and Wallace, 1993); (2) partitioning methods (Michelangeli et al. 1995, hereafter MVL); (3) probability density function (pdf) or "bump-hunting" methods (Kimoto and Ghil 1993a; Kimoto and Ghil 1993b; Corti et al. 1999); and (4) mixture model methods (McLachlan and Basford 1988; Haines and Hannachi 1995; Smyth et al. 1999). In the hierarchical approach, one iteratively builds a classification tree, starting from the individual data points, merging them into clusters according to a similarity criterion. The partitioning method gathers data around randomly chosen seeds, classifies all states into a predefined number of clusters, and iteratively finds the partition maximizing the ratio of the variance between cluster centroids

(averages over the states within a cluster) to the variance within clusters. The pdf method defines a regime in terms of the state vectors of maps or points in the large-scale atmosphere's state space which lie in the vicinity of a pdf maximum. The mixture model approach, unlike the previously used approaches, is based on an explicit, fully consistent probabilistic model.

These methods have all been applied to study the Northern Hemisphere winter variability, and in most cases have made use of a reduced dimensional representation of the full atmospheric phase space. In general none of the methods lead to a unique choice for the most probable number of clusters, and we found this to be the case for our analysis. However, several statistical approaches to estimating the significance of various cluster numbers have been formulated. Cheng and Wallace (1993) tested the reproducibility of their results for a given cluster number by repeating the analysis with many randomly chosen (sub-sampled) half-length data sets. In addition to reproducibility, MVL utilized a classifiability index, based on the correlation between the cluster centroids obtained from a very large number of different initial seeds. We will also use the significance of the clusters vis-a-vis those obtained from appropriate red-noise procceses, and the consistency of clusters using different variables as further tests in order to more narrowly define the most probable number of clusters. For most years we will be able to narrow the range of cluster number. The identity of the most important pattern we find, as well as its dependence on time scale, are not sensitive to which cluster number within this range is chosen.

(b) Partitioning Cluster Technique. In this paper we utilize the partitioning method of MVL. This method identifies clusters in the reduced phase space defined by the empirical

orthogonal functions (EOFs), with the associated principal components (PCs) providing the new coordinates. For a given number of clusters k, the optimum partition of data into k clusters is found by an algorithm which takes an initial cluster assignment (based on the distance from pseudo-random seed points), and iteratively changes it by assigning each element to the cluster with the closest centroid, until a "stable" classification is achieved. (A cluster centroid is defined by the average of the PC coordinates of all states which lie in that cluster.) This process is repeated 100 times (using different seeds), and for each partition the ratio of variance among cluster centroids (weighted by the population) to the average intra-cluster variance is recorded. The cluster partition which yields the maximum variance ratio is selected as the reference partition. Note that the variances depend on which norm is used; we use the Euclidean norm in the phase space of 200 hPa height. But we also carried out the cluster analysis using zonal wind, which corresponds to carrying out the analysis with the height field but with a different norm. We shall return to this point.

(c) Significance. The significance of the clustering for given cluster number k can be assessed compared to a multi-variate red noise synthetic data set. The red-noise data are generated by assuming a Markov (first order auto-regressive) process for each PC, with the same variance and lag-one covariance found from the GCM data. 100 sets of synthetic data are generated (each as long as the GCM record for each winter), and the cluster analysis applied to each. The percentage of cases p for which the red-noise data yield a higher variance ratio than the GCM data is obtained, and the significance level assessed as $(100 - p)$.

Table 2 shows the significance level for 200 hPa height as a function of cluster number

k for each year separately. Levels of 90 percent or higher are listed in bold type. Also listed are tropical Pacific SST Niño3 and Niño3.4 indices for the months of Dec.-Feb. (DJF), as well as the time series of with the model simulated SST forced signal in the seasonal mean. (The forced signal is defined as the leading EOF of the 18-winter time series of the ensemble/seasonal means. See the Appendix for details.) For three out of the four warmest events (as defined by the SST indices: 1982/93, 1986/87 and 1997/98) the significance levels are quite low, and none exceed (or even come close to) the 90 percent level. Further, the one exception (1991/92) is not a strong warm event based on the model response, that is the GCM does not respond to the SST anomalies in this year as in other warm years. The remaining (normal and cold) winters are not readily distinguishable from each other based on this measure of significance. Two of the winters, 1981/82 and 1987/88 have a narrower range of cluster numbers which are significant.

Table 3 shows the ratio of centroid variance to intra-cluster variance for cluster numbers 2 to 6, averaged over the 18 winters considered. On average, a four-cluster partition yields a variance ratio greater than one, indicating that the cluster centroids account for more than half of the total PC variance. Values for individual years (not shown) indicate that only during warm ENSO events is a partition into more than 4 clusters needed to cross this threshold.

Table 4 shows the serial correlation between the variance ratio and the two (DJF) SST indices, as well as between the variance ratio and the SST forced signal, for varying cluster number k. (The higher the variance ratio, the stronger the clustering.) The strong negative

correlations (generally below -0.80) between the SST indices and the variance ratio, and between the SST forced signal and the variance ratio, are in part attributable to the behavior of the El Niño events. Two aspects of these results are worth noting: (a) The correlations of SST indices with the variance ratio are nearly as strong as those with the PC of the SST forced signal; (b) Strong El Niño events do not result in flow regime behavior; otherwise, regime behavior is commonly seen. Point (a) is further illustrated in Figure 4, which shows scatter plots of the leading signal PC vs. DJF Niño3 (panel a), the 3-cluster variance ratio vs. DJF Niño3 (panel b), and the 3-cluster variance ratio vs. the signal PC (panel c).

The relationship between the cluster variance and the seasonal mean SST is as strong as that between the seasonal mean forced response and the SST. This remarkable result shows the strong influence of ENSO on the *structure* of intra-seasonal variability.

(d) Reproducibility. We tested the reproducibility of the clusters by computing the reference partition of 200 hPa height for 100 random sub-samples, each containing half the atmospheric data in any given 55 member ensemble. The average anomaly correlation between the cluster centroids of the random sub-samples and the best-match centroids of the original reference partition provides a reproducibility index, as in MVL.[2] Averaged over all 18 winters, this index is 1.00 for k=2, 0.98 for k=3 and 0.97 for k=4-6. Averaged over all values of k between 2 and 6, the index is 0.97 or above for all winters other than the El-Niño winters of 1982/83 and 1997/98. The high reproducibility of the results does not provide a basis for further restricting the number of clusters.

[2]All averages of correlations are taken using the Fisher z-transform (see Snedecor and Cochran, p 185.)

(e) Dynamic Consistency. The entire set of cluster calculations was repeated using the 200 hPa u-wind in place of the 200 hPa height field. (Note that since geostrophic balance holds to a good approximation in mid-latitudes, this can be thought of as a calculation of clusters using a metric in which the squared distance between two points in phase space is taken to be the sum of squared differences of the meridional derivative of height.) If the clusters correspond to physical weather regimes, they should be accessible using u-wind as well as height field, or put another way, should be relatively independent of the distance metric used.

We compared the geostrophic zonal wind u_g maps based on the centroid maps of the height cluster calculations with the centroid maps of the zonal wind u calculation, and determined whether a one-to-one matching could be made (for any given cluster number k) between the two sets of clusters. This was accomplished by computing the u cluster centroid which was closest (in terms of pattern correlation) to each of the k u_g centroids. If each u centroid was picked once and only once, the matching was one-to-one. For those k for which we obtained such matching, we computed the average correlation between the cluster centroids. If for any k (and for any winter) the cluster matching was not one-to-one, or if the average correlation between matched centroids was less than 0.80, we eliminated that cluster number as being a probable candidate. The table of surviving possible cluster numbers (Table 5) shows that we were not successful in limiting k to one and only one value for each of the 15 years, the warm events having been already eliminated. For many years a range of clusters remains, with k=3 and k=4 appearing for 13 out of the 15 years.

In the rest of the paper, we refer to the cluster partitions with numbers k appearing in Table 5 as having generalized significancee

5. Flow Regimes.

(a) Properties and Paterns of Flow Regimes. In this section we present maps of the weather regimes of the 200 hPa height field. They will be presented both as anomalies from the long-term climatological seasonal mean, and as total fields. In order to provide a logical ordering of the clusters, we note that the temporal variance of the field Y, which is the total height field on time scales longer than 10 days, but with the ensemble mean annual cycle removed (see section 3), can be written as:

$$V = \frac{1}{N}\sum_{t=1}^{N}\left(Y(t)\right)^2 = \frac{1}{N}\sum_{t=1}^{N}\sum_{r=1}^{k}\left(\left[Y_r(t)\right]^2\right) \tag{6}$$

where $Y_r(t)$ is the value of Y at time t when the system is in cluster r, and is zero if the system is in any other cluster. Since any given ensemble member for any given time is in only one cluster, the above equation allows us to write the total variance as a sum of variances due to each cluster. (It is understood that V is to be also averaged over ensemble members for a given winter.) Finally, taking the spatial average of V over the whole domain considered gives a single variance measure which is used to rank the clusters, the first having the largest variance, and so on.

(b) Regime Maps for 200 hPa Height. Figures 5 - 7 show the clusters (regimes) in 200 hPa height for k=3 for 6 out of the 13 winters for which k=3 has generalized significance. In all cases we show the mean of all states in the cluster, expressed both as the total height

field (light solid contours) and the anomaly with respect to the 18-winter mean climatology (heavy solid contours). The time spent in each cluster (expressed as a fraction of the total season) is given in parentheses in the figures.

The first regime for 1983/84 shows a wavetrain - like character with a substantial enhanced ridge centered over the Aleutians (anomaly exceeding 300 m), a trough extending from the southwest to northeast centered on central Canada, and a weaker ridge over the Southeast U.S. The second regime is associated with much weaker anomalies, and has a structure similar to the first, but with opposite polarity. The third regime has the amplified ridge directly over the northwestern coast of North America. The first regime for 1998/99 (a strong La Niña year) is nearly identical to Regime 1 for 1983/84, only with an even larger anomaly (ridge exceeding 350 m). The large amplitude planetary wave flow of this regime contrasts to the much more zonal flow of the second regime, whose anomalies are considerably weaker. The third regime has a structure which is quite similar to the SST forced signal derived from the ensemble seasonal means (see the Appendix) but with opposite phase.

Figures 6 and 7 show the regimes for k=3 for the winters of 1991/92, 1994/95, 1984/85 and 1996/97. (The six winters in Figures 5-7 were chosen more or less randomly from Table 5, although we did want to include a few cold La Niña events.) In all the winters shown, and in all the other 7 winters for which k=3 has generalized significance, one of the clusters corresponds fairly closely to the first regime of 1983/84 and 1988/89. We term this the Alaskan ridge (AR) pattern. This pattern is always one of the first two regimes, occurs with varying strength, and occurs roughly 20 to 25 percent of the time for $k = 3$. The strongest

ridge is during 1988/89 (over 350 m anomaly), the weakest during 1991/92 (150 m anomaly).

In comparing regimes for different winters, it is important to keep the number of regimes k constant, because as k increases, the average anomalies tend to increase, and the fraction of time spent in each cluster tends to decrease. Figures 8 and 9 show the regimes for k=5 for the winters 1981/82 and 1996/97, for which five clusters have generalized significance. For both winters the leading regime bears a strong resemblance to the AR pattern, and in 1996/97 another regime (3) has a fairly similar structure. For this year k=3 and k=4 are significant, in which cases clusters 1 and 3 merge to form a single cluster (not shown).

It is noteworthy that the same AR pattern also appears for cluster numbers which are not considered significant. This is illustrated in Figure 10, which shows results for the winter for 1990/91 for k=2 (not significant) and k=4 (significant). The AR pattern appears relatively unchanged in both sets, the only difference being the strength of the Alaskan anomaly (over 350 m for k=4, 250 m for k=3).

In summary, the AR pattern seems to be a preferred flow regime in all normal and cold ENSO winter circumstances.

(c) Winter of 1991/92. It was noted in discussing Table 2 that the winter 1991/92 seemed to be the exception among warm (El Niño) winters, for it does exhibit significant clustering. While this winter is associated with large Pacific SST indices, the GCM's forced response for this winter was rather weak. (The forced response is measured by the PC of the leading EOF of ensemble-seasonal means, as discussed in the Appendix.) Figures 6a and 6b shed some insight into this, for the second regime bears some resemblance to the forced signal

shown in the Appendix, with low anomalies over the Gulf of Alaska and high anomalies over northeastern Canada. There are differences between the second regime and the ENSO signal, particularly in the location of the anomalous Pacific low. Nevertheless, Figure 6b does suggest that the GCM is responding to the equatorial Pacific SSTs in this winter, but that this response must compete with the AR pattern (Figure 6a).

(d) Variance of AR Regime. The variance due to the AR regime alone, integrated over the North Pacific region of $160^oE - 210^oW, 40^oN - 80^oN$ is shown in Figure 11, which is comparable to Figure 3. Comparing Figure 11b with Figure 3b, we see that the AR pattern is responsible for about 40 percent of the total winter variance. Comparing the time series of North Pacific area-integrated variance, the largest negative deviations seen in Figure 3a are not plotted in Figure 11a, since they correspond to the three warm Pacific events for which no clusters were significant. Some of the more moderate extrema in Figure 3a (minimum in 1991/92, maxima in 1984/85 and 1996/97) are also seen in Figure 11a. The AR region variance is only modestly correlated with with the ENSO indices, with correlation values of -0.40 and -0.49 for Niño-3 and Niño-3.4, respectively.

(e) Typical AR Regime Lifetime. The lifetime of a cluster refers to the number of consecutive days in which the low frequency time series $Y(t)$ is identified as being in that cluster before it moves to a different one. The lifetimes depend on the cluster number k and on the cluster itself. In Table 6 we show the average lifetime (in days) of the AR pattern for k=3 as well as the maximum lifetime for each of the 15 winters for which clustering is significant. While the average lifetime is relatively short, between 10 and 15 days, the maximum lifetime

ranges from 36 to 78 days, indicating that for at least one ensemble member in each winter the AR pattern can be very persistent.

6. The AR Pattern and Seasonal-Mean Climate Noise.

The AR pattern corresponds to one of the clusters (regimes) in every case of generalized significance (each non-blank entry in Table 5.) Its spatial pattern very strongly resembles the leading climate noise pattern shown in Figure 15. (The climate noise pattern is obtained as the leading EOF of the deviation of seasonal means about the ensemble seasonal means for all 18 winters.) This strong similarity suggests that the leading ($i = 1$) term in the expansion:

$$Y(t) = \sum_{i=1}^{i=3} (C_i - \langle C_i \rangle)\ P_i(t) + X_L(t) \tag{7}$$

based on equation 5 dominates the entire analysis for each winter. One hypothesis is that the appearance of the AR pattern in the individual time series $Y(t)$ is only due to the intra-ensemble variability of the seasonal mean; the AR pattern has nothing intrinsically to do with variability within the season.

An alternative hypothesis is that this preferred regime corresponds to a physical state which occur on a variety of intra-seasonal time scales, and since the AR regime tends to have larger amplitude anomalies compared to the other regimes it leaves its imprint on the seaonal mean. In this view the seasonal-mean climate noise is just the statistical residue of intra-seasonal regime behavior.

In order to distinguish between these hypotheses, we have repeated the entire cluster analysis using only the low frequency field $X_L(t)$ for each winter. This corresponds to

subtracting not the ensemble mean annual cycle but the estimate of the annual cycle made for each seasonal simulation individually. If the same regime patterns occur in this calculation as seen previously, this would strongly support the view that the regimes are intriniscally intra-seasonal phenomena.

The significance against simulated red-noise data is shown in Table 7, which can be compared to Table 1. It is clear that the overall level of significance is lower, with only 9 years showing levels above 90 percent for any cluster number k. Figures 12-14 show the regime averages for the case k=3 for the same years as seen in Figures 5-7, in precisely the same format. Note that according to Table 7 the clustering has no significance for k=3 for the winters of 1983/84 and 1991/92, marginal significance for 1996/97, while significance is seen for the remaining three winters (1984/85, 1988/89, and 1994/95).

Yet comparing Figures 12-14 with Figures 5-7 it is very striking that the regime anomalies have precisely the same pattern. Removing the ultra-low frequency components of the height field has reduced the magnitude of the regime anomalies but left their structure unchanged. This conclusion holds for all 15 winters for which clustering has generalized significance, strongly indicating that the regimes identified by the clustering algorithm are robust preferred states.

The lowered significance of the low frequency only clusters can be understood as follows: The ultra-low frequency components alone are expected to have a nearly Gaussian pdf on the basis of the Central Limit Theorem. Hence subtracting these components from the full

time series (which has a non-normal pdf) will tend to mask multi-modality.

7. Summary, Discussion and Conclusions.

In this work we study all time scales longer than 10 days in 55-member ensembles of GCM seasonal simulations for 18 winters. Each ensemble uses specified observed weekly SSTs as boundary conditions.

We emphasize the distinction between intra-seasonal fluctuations containing periods of 10 days to a season (low frequency) and the ultra-low frequency fluctuations. The latter are expressed as the sum of the seasonal mean, seasonal trend and a best-fit parabola (also see Straus 1983). The intra-ensemble variability in the ultra-low frequency components represents variability about which prior knowledge of SST tells us nothing; it is due to internal dynamics. Yet this component of variability is not always explcitly recognized. In the Pacific North-American region it contributes as much as the low frequency variance (compare Figures 3 and 2).

With the ensemble mean seasonal cycle removed, both low frequency and ultra-low frequency variability is retained in the cluster analysis that is separately applied to each of the 18 winters.

The results for the Pacific - North American region ($150^oE - 30^oW$, $20^oN - 80^oN$) show that for all winters except the El Niño winters of 1982/83, 1986/87 and 1997/98, the COLA GCM shows a significant tendency to form clusters, or regimes. While it is not always possible to precisely determine the most probable number of clusters k, the clusters are significant with respect to (a) synthetic red-noise simulations using the same variance and

lag-one correlation as the original PCs, (b) reproducibility of half-length samples, and (c) consistency with clusters determined independently from the 200 hPa height and zonal wind fields.

One cluster which appears for all 15 significant years, and for all significant choices of k, consists of a relatively strong amplified ridge over southern Alaska, a northeast-soutwest oriented trough over much of the central North American continent, and a weaker high over Florida. This Alaskan ridge (AR) pattern was also found in observations by Kimoto and Ghil (1993b,b) (their PAC regime 2), by Corti et al. (1999) (their cluster B), and by Cheng and Wallace (1993) (their pattern A). Note that these observational studies show substantial agreement in terms of significant clusters, even though they used slightly different periods, different levels (700 hPa, 500hPa and 200 hPa), different regions (regional and hemispheric), different nominal data truncations (2 PCs vs. no truncation), and different clustering methods (pdf methods vs. hierarchical algorithm). The agreement between these observational studies and the GCM results found here is quite encouraging, both with respect to the realism of the GCM and the significance of the regimes. (MVL also study regional clusters, but their choice of regions makes comparison difficult.)

More problematic is reconciling our results, and the previously cited observational results, with those of Toth (1991, 1993b,a). In these studies the data are pre-filtered to retain only quasi-stationary (slowly varying) anomalies, and the clustering algorithm seeks regions in the full phase space which are significantly more (or less) populated than a full multi-normal distribution. Three winter clusters are found which do not convincingly match those

described in the previously mentioned observational studies. These clusters are most likely to be seen during months in which the tropical Pacific SST are *above* normal. Apparently this particular approach to regimes does not filter out smaller scales, as witnessed by small scale features shown in the clusters shown in Toth (1993a), and the resulting large number of degrees of freedom may be too large for the available sample (see e.g. Kimoto and Ghil 1993a; Silverman 1986).

The dominant AR pattern also appears to characterize the seasonal-mean climate noise, that is the intra-ensemble variability of seasonal means. (The leading EOF of all seasonal mean deviations about ensemble means for 18 winters reproduces the AR pattern. It explains 46 percent of the variance, and is significant.) This raises the question of whether the dominant regime seen in the cluster calculations for 15 winters is simply a reflection of the variability of the seasonal mean within ensembles, and whether it has anything to do with the traditional low-frequency fluctuations.

To answer this question, we have repeated the cluster calculations for all 18 winters retaining only the low frequency flow, so that all ultra-low frequency components (including the seasonal-mean climate noise) have been removed. While the significance levels for the clusters found in this calculation are much lower (and only exceed 90 percent for 9 winters), *the patterns corresponding to the flow regimes are unchanged.* This conclusion holds for all winters and for all cluster numbers for which the original clusters are significant.

These results provide a clear indication that the non-SST forced variability of seasonal means and ultra-low frequency components is a statistical residue of the occurrence of flow

regimes and transitions between them. These regimes show a wide range of residence times in individual realizations; the AR regime lasts for about 12-15 days on average, but can last for 40-70 days (Table 6). The implications are that the regime dynamics of the model atmosphere can influence the magnitude and characteristic patterns of something as basic as the uncertainty in the seasonal mean for given SST forcing.

This work can be seen as a generalization of the work of Compo et al. (2001) from the SST-dependence of local statistics (e.g. variance) to the SST-dependence of important flow regimes. That major warm El Niño events are categorically different than other years in this regard suggests that the associated tropical heating anomalies reorganize the mid-latitude circulation in the Pacific - North American region sufficiently to disrupt the normal regime behavior.

Although the results of this study hold only for the COLA GCM, the fact that qualitatively similar results on the relationship between ENSO and extratropical regimes were found by Molteni and Corti (1998) in simpler quasi-geostrophic simulations suggests a more general validity of our findings. Comparisons of regime behavior with other GCMs and new diagnoses of observed regimes are both highly desirable, and we plan to pursue them.

Acknowledgements. We wish to acknowledge the work of Larry Marx and Dan Paolino in executing the large number of GCM simulations. This work was supported by the National Science Foundation under grant ATM-98-14295, the National Aeronautics and Space Administration under grant NAG5-8208, and the National Oceanic and Atmospheric Administration under grant NA96-GP0056.

Appendix. SST-Forced Signal and Climate Noise. In order to derive a pattern which is characteristic of the leading SST-induced signal in the seasonal mean, we compute the EOFs of the series of 18 seasonal ensemble means for 200 hPa height, as in Straus and Shukla (2000, 2002). The leading EOF pattern is shown in Figure 15. It explains 65% of the variance, and therefore well separated from the second EOF (which explains 13%) according to the criterion of North et al. (1981).

Climate noise in the seasonal mean is defined here as the intra-ensemble variability of the seasonal mean. By examining the EOF expansion of the departures from the ensemble mean of all 990 seasonal means spanning 18 years, we obtain a set of patterns which are characteristic of the noise as a whole. The leading EOF is shown in Figure 16, and explains 43% of the variance. It is statistically distinct from the second EOF, which explains 19%.

Data	Niño3	Niño3.4
NCEP X_L	-0.65	-0.61
GCM X_L	-0.79	-0.75
GCM $X_U + X_L$	-0.84	-0.80

Table 1: Correlation of DJF Niño3 and Niño3.4 indices with observed low frequency variance, integrated over the region of $160^oE - 110^o$, $40^oN - 80^oN$, given in first row. Second row gives same correlations for GCM low frequency variation, third row for GCM total (low + ultra-low) variance.

Winter	k=2	k=3	k=4	k=5	k= 6	Nino3	Nino3.4	PC
1981/82	81	89	83	**91**	**91**	-0.50	-0.13	0.52
1982/83	68	45	57	42	54	2.21	1.89	2.10
1983/84	88	**100**	**98**	**98**	**99**	-0.50	-0.68	-0.51
1984/85	86	**95**	**93**	**98**	**100**	-1.09	-1.10	-0.84
1985/86	**91**	**100**	**99**	**100**	**100**	-0.75	-0.64	0.29
1986/87	61	67	52	70	74	0.60	0.84	1.49
1987/88	60	**97**	87	87	87	0.34	0.50	0.58
1988/89	**97**	**98**	**98**	**99**	**99**	-1.21	-1.60	-1.85
1989/90	89	**98**	**98**	**99**	**100**	-0.35	-0.16	-1.00
1990/91	**94**	**100**	**97**	**99**	**100**	-0.16	0.12	-0.70
1991/92	67	**93**	**91**	**92**	**92**	0.87	1.25	0.55
1992/93	85	**99**	**100**	**100**	**100**	-0.16	0.04	-0.13
1993/94	**100**	**99**	**99**	**100**	**100**	-0.14	-0.10	0.54
1994/95	83	**99**	**94**	**99**	**100**	0.43	0.65	-0.07
1995/96	86	**99**	**96**	**99**	**99**	-0.71	-0.83	-0.74
1996/97	**95**	**98**	**97**	**100**	**100**	-0.71	-0.51	-0.37
1997/98	35	25	36	70	74	2.29	1.76	1.40
1998/99	87	**92**	**97**	**94**	**97**	-0.90	-1.31	-1.25

Table 2: Significance p (in percent) of clusters against red-noise Markov model constructed using same variance and lag-one correlation of the leading four PCs of GCM data. k gives the cluster number. $p = 100 - e$, where e is the number of synthetic Markov data sets for which the ratio variance exceeds that of the GCM. Values of p over 90 are given in bold. Also shown are the standardized Niño3 and Niño3.4 indices, as well as the standardized leading PC of the seasonal ensemble means, i.e. the climate signal, (see the Appendix).

	k=2	k=3	k=4	k=5	k= 6
μ	0.506	0.813	1.082	1.319	1.536
σ	0.087	0.133	0.165	0.188	0.213

Table 3: Mean (μ) and standard deviation (σ) of variance ratio across 18 winters, as a function of cluster number k. The variance ratio is defined as the ratio of phase space variance between cluster centroids to the average intra-cluster variance. See text for details.

	k=2	k=3	k=4	k=5	k= 6
Niño3	-0.83	-0.87	-0.82	-0.83	-0.83
Niñ03.4	-0.81	-0.85	-0.80	-0.79	-0.80
PC-ENSO	-0.80	-0.86	-0.84	-0.84	-0.84

Table 4: Correlation between the DJF Niño3 index (top row) and the Niño3.4 index (middle row) and the variance ratios for k = 2 - 6. Bottom row gives correlation between the variance ratios and the PC of the seasonal ensemble mean, which gives the leading SST-forced signal (see Appendix).

Winter	k=2	k=3	k=4	k=5	k= 6
1981/82				Yes	Yes
1982/83					
1983/84		Yes	Yes	Yes	Yes
1984/85		Yes	Yes	Yes	Yes
1985/86		Yes	Yes		Yes
1986/87					
1987/88	Yes				
1988/89	Yes	Yes	Yes	Yes	
1989/90		Yes	Yes	Yes	Yes
1990/91		Yes	Yes	Yes	
1991/92		Yes	Yes		
1992/93		Yes	Yes	Yes	
1993/94	Yes	Yes	Yes	Yes	Yes
1994/95		Yes	Yes		
1995/96		Yes	Yes		
1996/97	Yes	Yes	Yes	Yes	
1997/98					
1998/99		Yes	Yes		

Table 5: Table of cluster numbers (k) for which the cluster results pass the tests of significance vis-a-vis synthetic red noise processes, reproducibility, and dynamical significance. See text for details.

Winter	Average	Maximum
1981/82	9.6	36
1983/84	14.6	56
1984/85	14.7	64
1985/86	10.8	36
1987/88	12.4	64
1988/89	13.6	68
1989/90	11.5	52
1990/91	12.4	68
1991/92	12.3	44
1992/93	13.0	76
1993/94	16.9	68
1994/95	10.5	32
1995/96	12.1	56
1996/97	15.7	52
1998/99	15.7	60

Table 6: Average and maximum lifetimes of clusters for k=3, in days.

Winter	k=2	k=3	k=4	k=5	k= 6
1981/82	81	76	71	62	62
1982/83	28	29	25	35	27
1983/84	24	56	61	74	70
1984/85	57	**90**	84	89	**91**
1985/86	78	**90**	85	84	85
1986/87	55	75	81	72	78
1987/88	38	84	**95**	82	**95**
1988/89	43	**90**	75	80	85
1989/90	77	81	88	**91**	**93**
1990/91	70	81	62	66	82
1991/92	45	43	53	58	62
1992/93	20	35	39	54	58
1993/94	27	64	50	27	48
1994/95	77	**92**	**92**	85	82
1995/96	42	72	63	**91**	84
1996/97	78	89	88	**93**	81
1997/98	48	66	61	64	70
1998/99	64	57	79	**92**	81

Table 7: Significance p (in percent) of clusters against red-noise Markov model for low frequency only data. (See text for explanation). Otherwise as in Table 2.

References

Branković, C. and T. N. Palmer, 2000: Seasonal skill and predictability of ecmwf provost ensembles. *Quart. J. Roy. Meteor. Soc.,* **126**, 2035–2067.

Chang, Y., S. D. Schubert, and M. J. Suarez, 2000: Boreal winter predictions with the GEOS-2 GCM: The role of boundary focing and initial conditions. *Quart. J. Roy. Meteor. Soc.,* **126**, 2293–2323.

Chen, W. Y. and H. M. van den Dool, 1997: Asymmetric impact of tropical sst anomalies on atmospheric internal variability over the North Pacific. *J. Atmos. Sci.,* **54**, 725–740.

Cheng, X. and J. M. Wallace, 1993: Cluster analysis of the Northern Hemisphere wintertime 500-hPa field: Spatial patterns. *J. Atmos. Sci,* **50**, 2674–2696.

Compo, G. P., P. D. Sardeshmukh, and C. Penland, 2001: Changes of subseasonal variability associated with El Niño. *J. Climate,* **14**, 3356–3374.

Corti, S., F. Molteni, and T. N. Palmer, 1999: Signature of recent climate change in frequencies of natural atmospheric circulation regimes. *Nature,* **398**, 799–802.

Duchon, C., 1979: Lanczos filtering in one and two dimensions. *J. Appl. Meteor.,* **18**, 1016–1022.

Graham, R. J., A. D. L. Evans, K. R. Mylne, M. S. J. Harrison, and K. B. Robertson, 2000: An assessment of seasonal predictability using atmospheric general circulation models. *Quart. J. Roy. Meteor. Soc.,* **126**, 2211–2240.

Haines, K. and A. Hannachi, 1995: Weather regimes in the Pacific from a GCM. *J. Atmos. Sci.,* **52**, 2444–2462.

Kalnay, E. and coauthors, 1996: The NCEP/NCAR 40-year reanalysis project. *Bull. Amer. Meteor. Soc.,* **77**, 437–472.

Kiehl, J. T., J. J. Hack, G. Bonan, B. A. Boville, D. L. Williamson, and P. J. Rasch, 1998: The National Center for Atmospheric Research Community Climate Model: CCM3. *J. Climate,* **11**, 1131–1149.

Kimoto, M., 1989. *Multiple flow regimes in the Northern Hemisphere winter. Ph.D. Thesis.* Los Angeles: University of California.

Kimoto, M. and M. Ghil, 1993a: Multiple flow regimes in the Northern Hemisphere winter. Part I: Methodology and hemispheric regimes. *J. Atmos. Sci,* **50**, 2625–2643.

Kimoto, M. and M. Ghil, 1993b: Multiple flow regimes in the Northern Hemisphere winter. Part II: Sectorial regimes and preferred transitions. *J. Atmos. Sci,* **50**, 2645–2673.

Kumar, A., A. G. Barnston, P. Peng, M. P. Hoerling, and L. Goddard, 2000: Changes in the spread of the variability of the seasonal mean atmospheric states associated with ENSO. *J. Climate,* **13**, 3139–3151.

Kumar, A. and M. P. Hoerling, 1997: Interpretation and implications of observed Inter-El Niño variability. *J. Climate,* **10**, 83–91.

Lorenz, E. N., 1964: The problem of deducing the climate from the governing equations. *Tellus,* **16**, 1–11.

McLachlan, G. J. and K. E. Basford, 1988. *Mixture Models: Inference and Applications to Clustering.* New York: Marcel Dekker.

Michelangeli, P.-A., R. Vautard, and B. Legras, 1995: Weather regimes: Recurrence and quasi-stationarity. *J. Atmos. Sci.,* **52**, 1237–1256.

Molteni, F. and S. Corti, 1998: Long-term fluctuations of the statistical properties of low-fequency variability: Dynamical origin and predictability. *Quart. J. Roy. Meteor. Soc.,* **124**, 495–526.

Moorthi, S. and M. J. Suarez, 1992: A parameterization of moist convection for general circulation models. *Mon. Wea. Rev.,* **210**, 978–1002.

North, G. R., T. L. Bell, R. F. Cahalan, and F. J. Moeng, 1981: Sampling errors in the estimation of empirical orthogonal functions. *Mon. Wea. Rev.,* **110**, 699–706.

Reynolds, R. W. and T. M. Smith, 1994: Improved global sea surface temperature analyses using optimal interpolation. *J. Climate,* **9**, 840–858.

Sardeshmukh, P. D., G. P. Compo, and C. Penland, 2000: Changes of probability associated with El Niño. *J. Climate,* **13**, 4268–4286.

Schneider, E. K., 2002: Understanding differences between the equatorial pacific as simulated by two coupled GCMs. *J. Climate,* **15**, 449–469.

Schubert, S. D., M. J. Suarez, Y. Chang, and G. Branstator, 2001: The impact of ENSO on extratropical low-frequency noise in seasonal forecasts. *J. Climate,* **14**, 2351–2365.

Shukla, J., J. Anderson, D. Baumhefner, C. Brankovic, Y. Chang, E. Kalnay, L. Marx, T. Palmer, D. Paolino, J. Ploshay, Schubert, D. Straus, M. Suarez, and J. Tribbia, 2000: Dynamical seasonal prediction. *Bull. Amer. Meteor. Soc.,* **81**, 2593–2606.

Shukla, J., D. A. Paolino, D. M. Straus, D. DeWitt, M. Fennessy, J. L. Kinter, L. Marx, and R. Mo, 2000: Dynamical seasonal prediction with the COLA atmospheric model. *Quart. J. Roy. Meteor. Soc.,* **126**, 2265–2291.

Silverman, B. W., 1986. *Density Estimation for Statistics and Data Analysis.* London: Chapman and Hall.

Smyth, P., K. Ide, and M. Ghil, 1999: Multiple regimes in Northern Hemisphere height fields via mixture model clusstering. *J. Atmos. Sci.,* **56**, 3704–3723.

Straus, D. M., 1983: On the role of the seasonal cycle. *J. Atmos. Sci.,* **40**, 303–313.

Straus, D. M. and J. Shukla, 1997: Variations of midlatitude transient dynamics associated with ENSO. *J. Atmos. Sci.,* **54**, 777–790.

Straus, D. M. and J. Shukla, 2000: Distinguishing between the SST-forced variability and internal variability in mid latitudes:Analaysis of observations and GCM simulations. *Quart. J. Roy. Meteor. Soc.,* **126**, 2323–2350.

Straus, D. M. and J. Shukla, 2002: Does ENSO force the PNA? *J. Climate,* **128**, 2340–2358.

Toth, Z., 1991. The effect of tropical SST on multiple equilibria in the NH extratropical circulation phase space. In *Preprints. Fifth Conf. on Climate Variations*, pp. 429–432. Amer. Meteor. Soc.

Toth, Z., 1993a: Preferred and unpreferred circulation types in the Northern Hemisphere wintertime phase space. *J. Atmos. Sci.,* **50**, 2868–2888.

Toth, Z., 1993b. Preferred extratropical circulation types: ENSO-induced or intrinsic? In *Proceedings of the Eighteenth Annual Climate Diagnostics Workshop*, pp. 171–174. Amer. Meteor. Soc.

Trenberth, K. E. and J. W. Hurrell, 1994: Decadal atmosphere-ocean variations in the pacific. *Climate Dyn.,* **9**, 303–319.

Xue, Y.-K., P. J. Sellers, J. L. Kinter, and J. Shukla, 1991: A simplified Biosphere Model for global climate studies. *J. Climate,* **4**, 345–364.

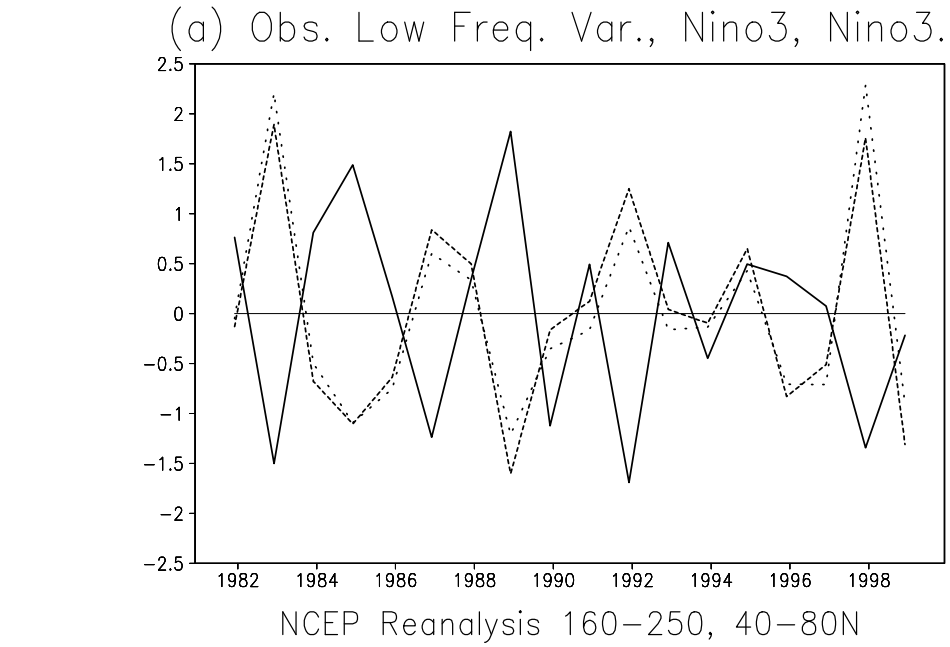

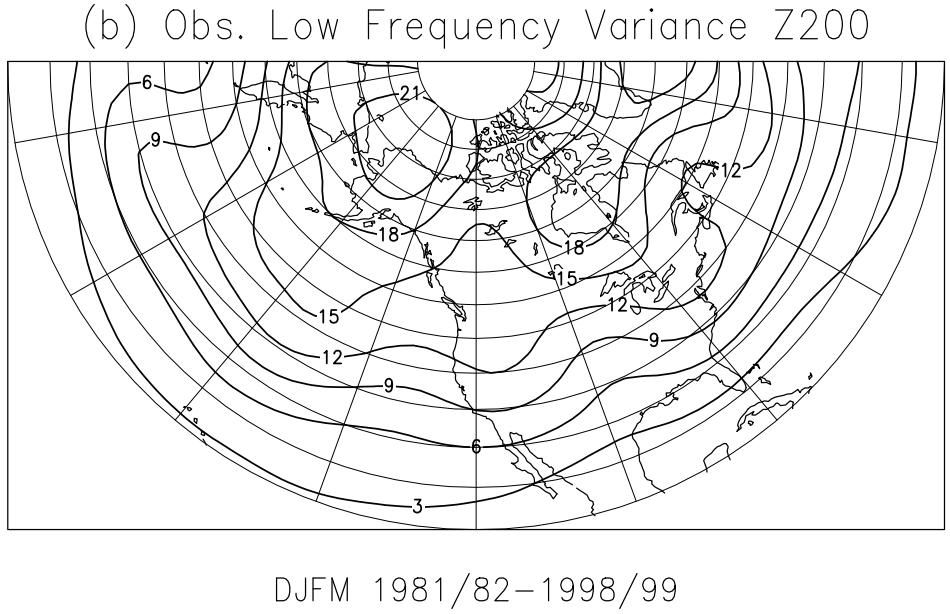

Figure 1: Low Frequency variance of 200 hPa height from NCEP reanalyses for the winters of 1981/82 through 1998/99. (a) Variance integrated over the North Pacific region $160^oE - 110^oW$, $40^oN - 80^oN$ (solid curve), Niño-3 index (dotted curve), Niño-3.4 index (dashed curve). (The indices are for the period of Dec.-Feb.) (b) Map of mean low frequency variance. Contour interval is 3000 m^2.

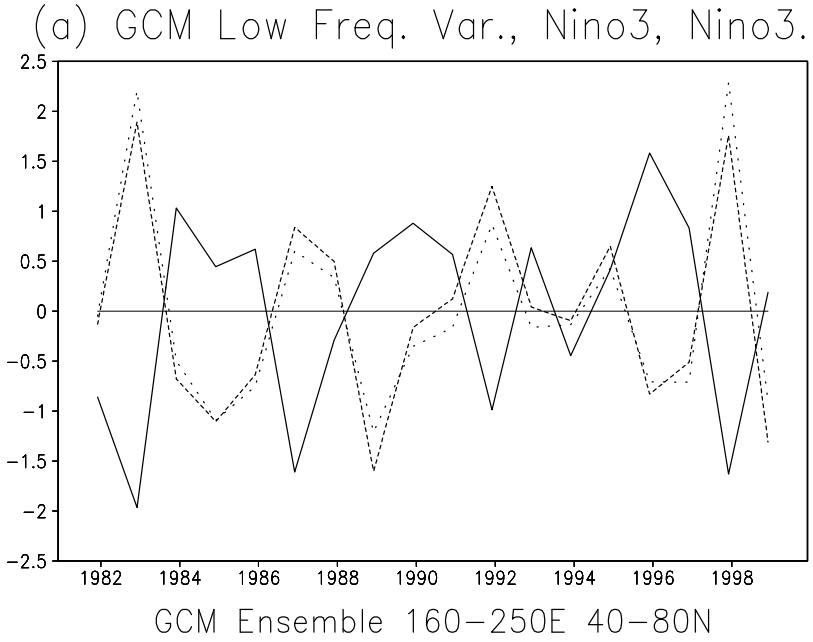

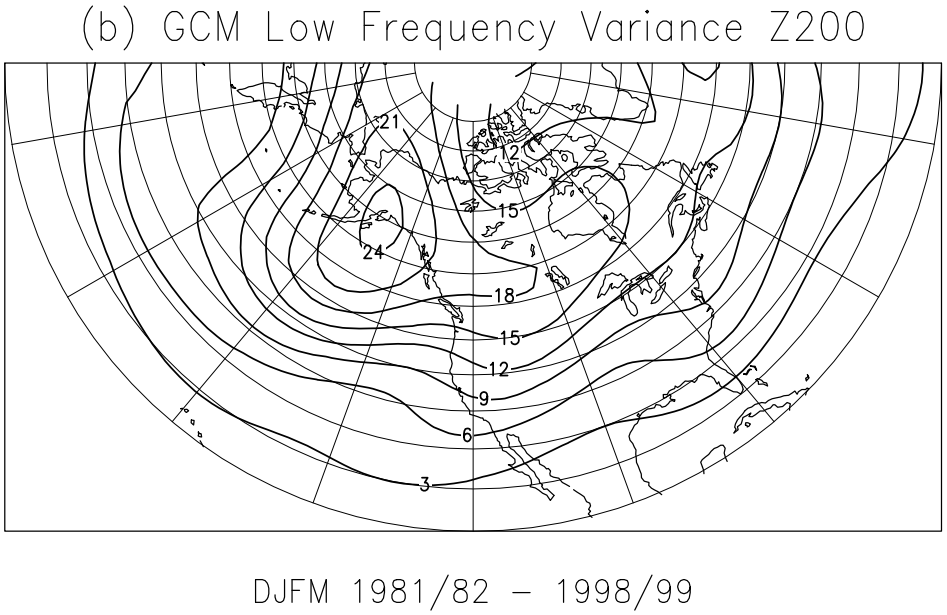

Figure 2: As for Figure 1, but for low frequency from GCM ensemble simulations.

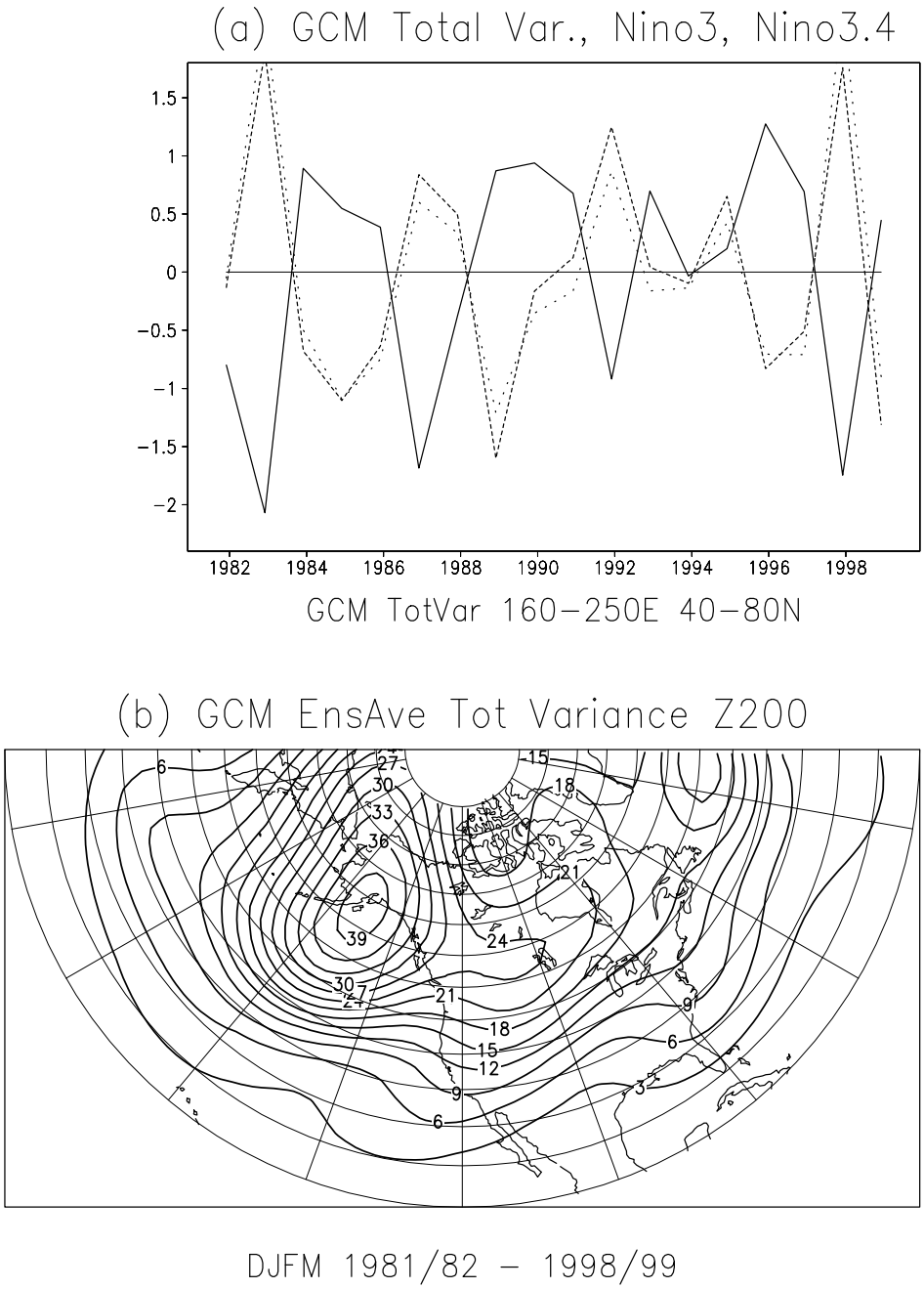

Figure 3: As for Figure 1, but for low frequency plus ultra-low frequency variance from GCM ensemble simulations. The ultra-low frequency variance includes the intra-ensemble variance of seasonal means and seasonal cycle. See text for details.

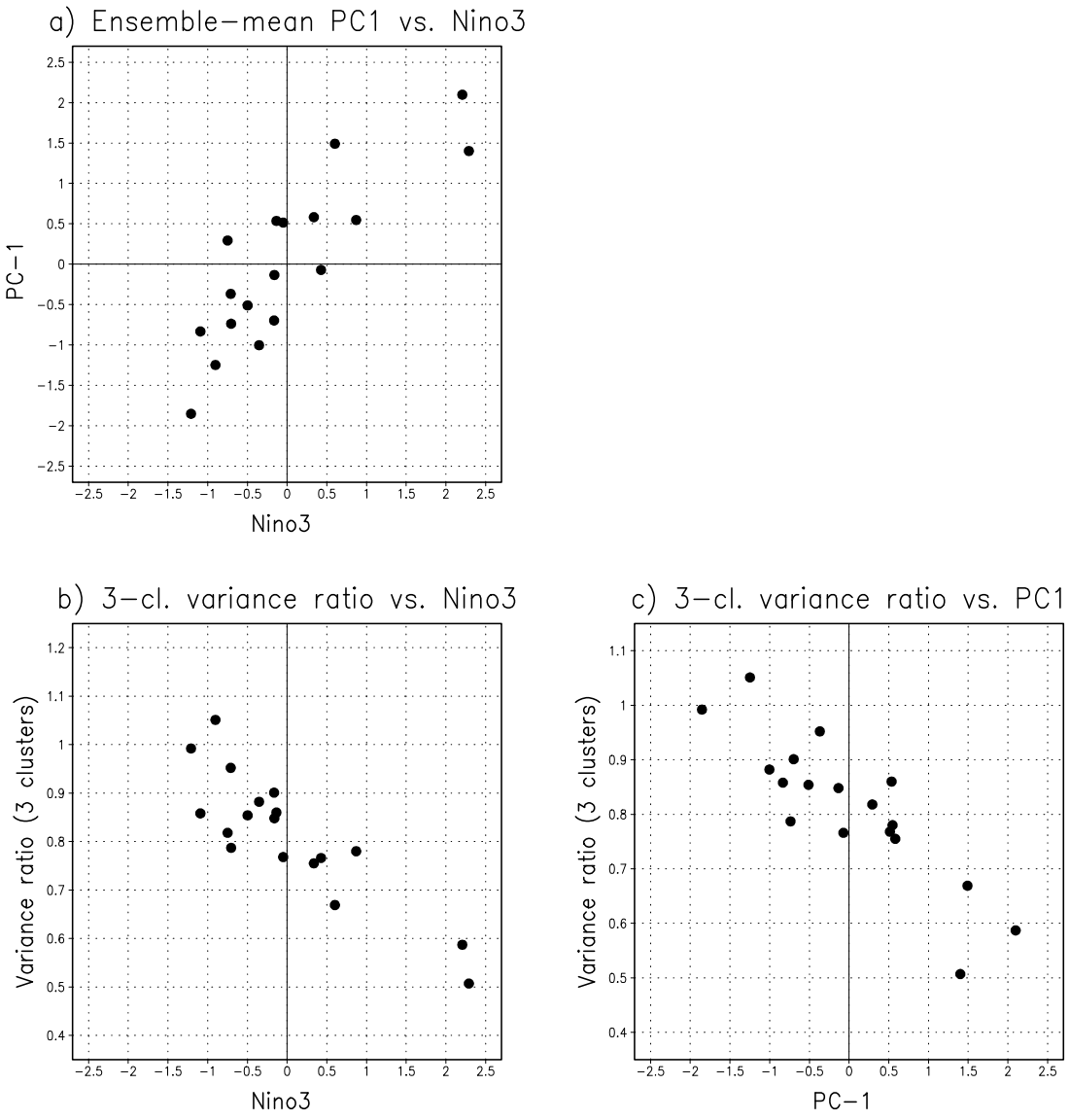

Figure 4: Scatter plots of the leading PC of ensemble/seasonal means vs. the DFJ Niño3 SST index (panel a), the 3-cluster (k=3) variance ratio vs Niño3 (panel b), and the 3-cluster variance ratio vs. the leading PC of ensemble/seasonal means. The leading PC and SST index time series are standardized.

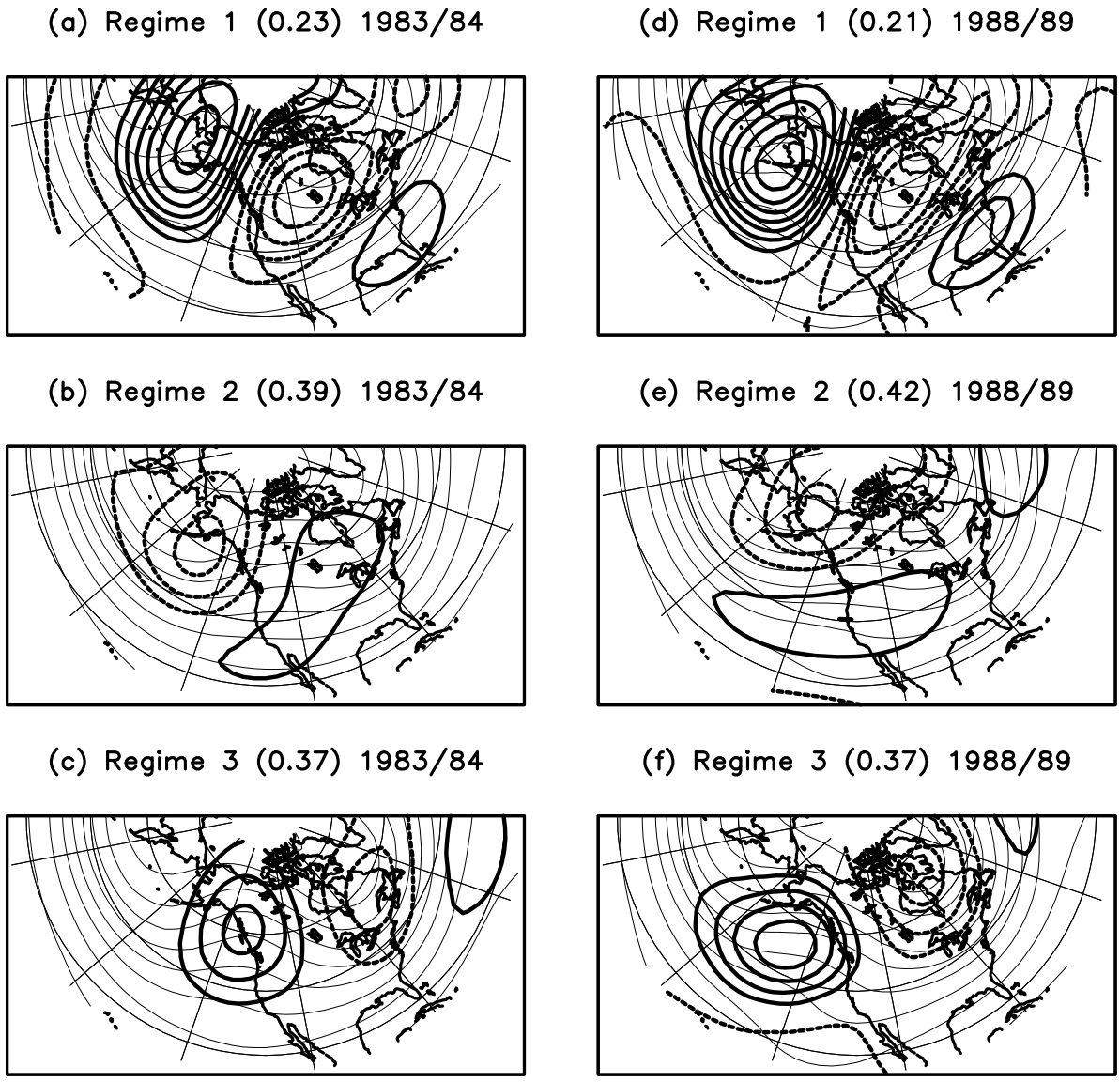

Figure 5: Average 200 hPa height for k=3 regimes. Light solid lines are total height, with a contour interval of 200 m, dark solid lines are anomalies with respect to GCM climate, with contour interval of 50 m. (Negative anomalies indicated by dark dashed lines.) (a)-(c), Regimes 1-3 for winter of 1983/84, (d)-(f), Regimes 1-3 for winter of 1988/89. Regimes are ordered by the area integral of the variance. The relative fraction of the regime residence is provided on the figure by the number in parenthesis (see text for explanation).

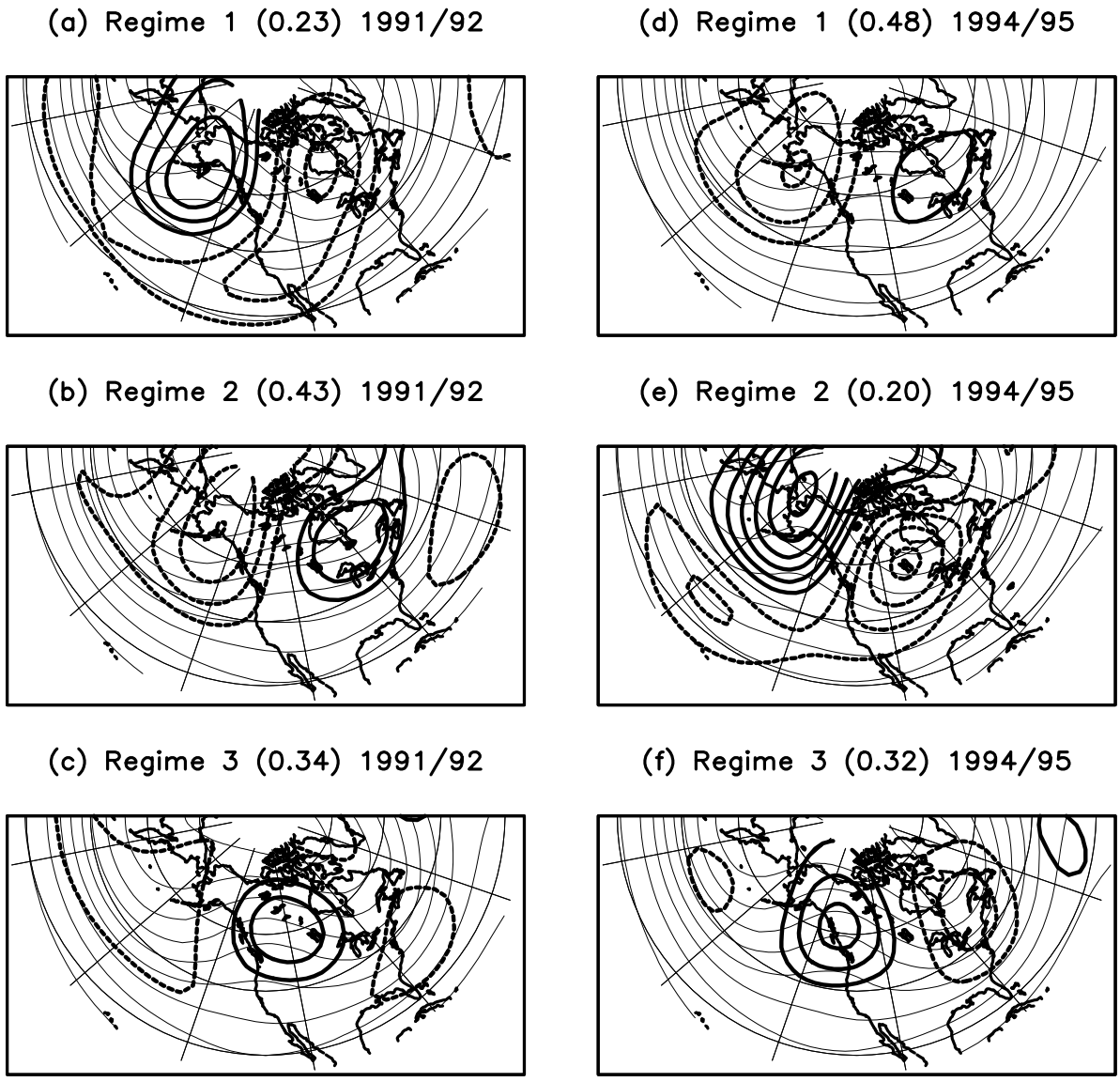

Figure 6: Average 200 hPa height for k=3 regimes. Light solid lines are total height, with a contour interval of 200 m, dark solid lines are anomalies with respect to GCM climate, with contour interval of 50 m. (Negative anomalies indicated by dark dashed lines.) (a)-(c), Regimes 1-3 for winter of 1991/92, (d)-(f), Regimes 1-3 for winter of 1994/95. Regimes are ordered by the area integral of the variance. The relative fraction of the regime residence is provided on the figure by the number in parenthesis (see text for explanation).

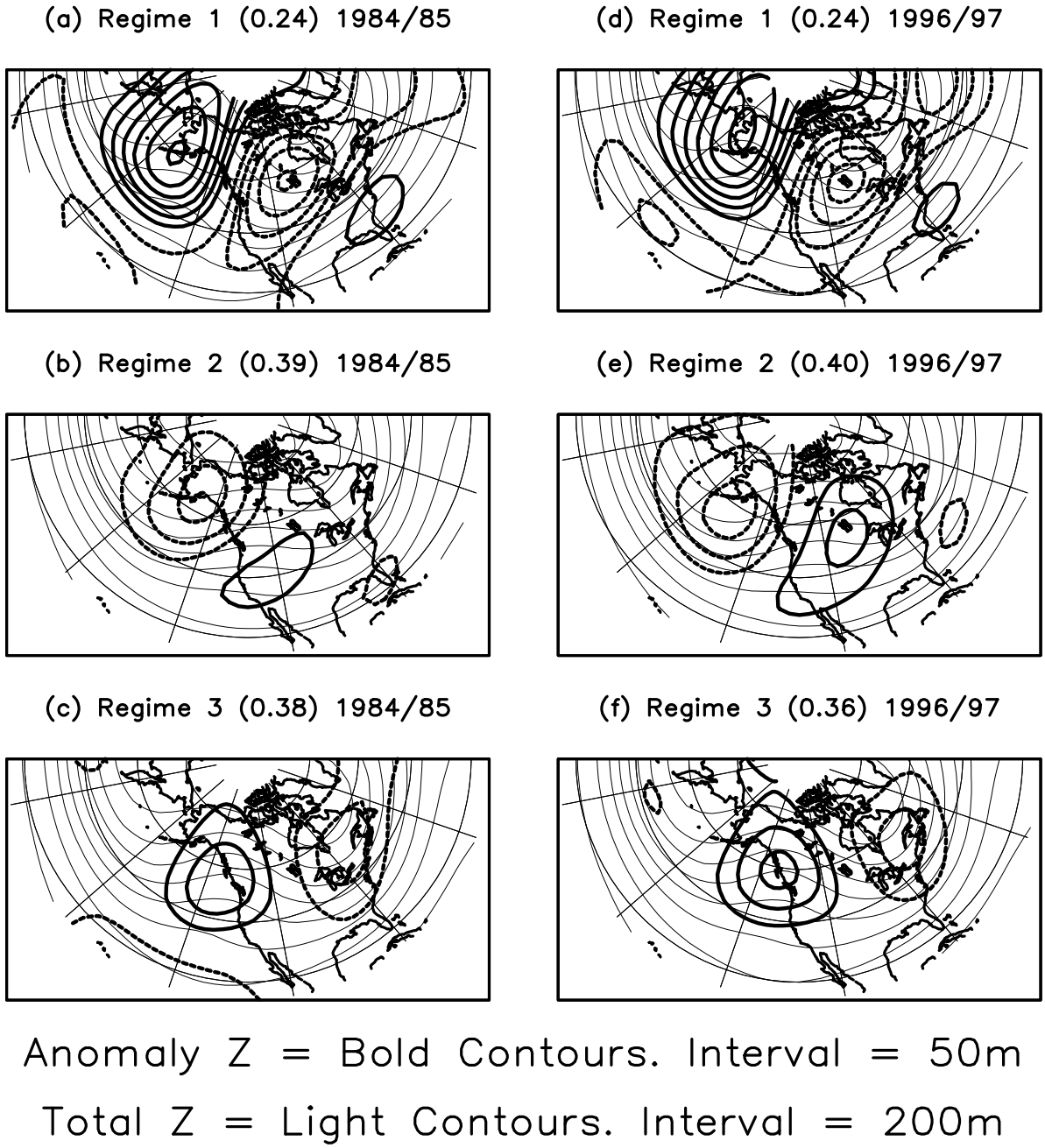

Figure 7: Average 200 hPa height for k=3 regimes. Light solid lines are total height, with a contour interval of 200 m, dark solid lines are anomalies with respect to GCM climate, with contour interval of 50 m. (Negative anomalies indicated by dark dashed lines.) (a)-(c), Regimes 1-3 for winter of 1984/85, (d)-(f), Regimes 1-3 for winter of 1996/97. Regimes are ordered by the area integral of the variance. The relative fraction of the regime residence is provided on the figure by the number in parenthesis (see text for explanation).

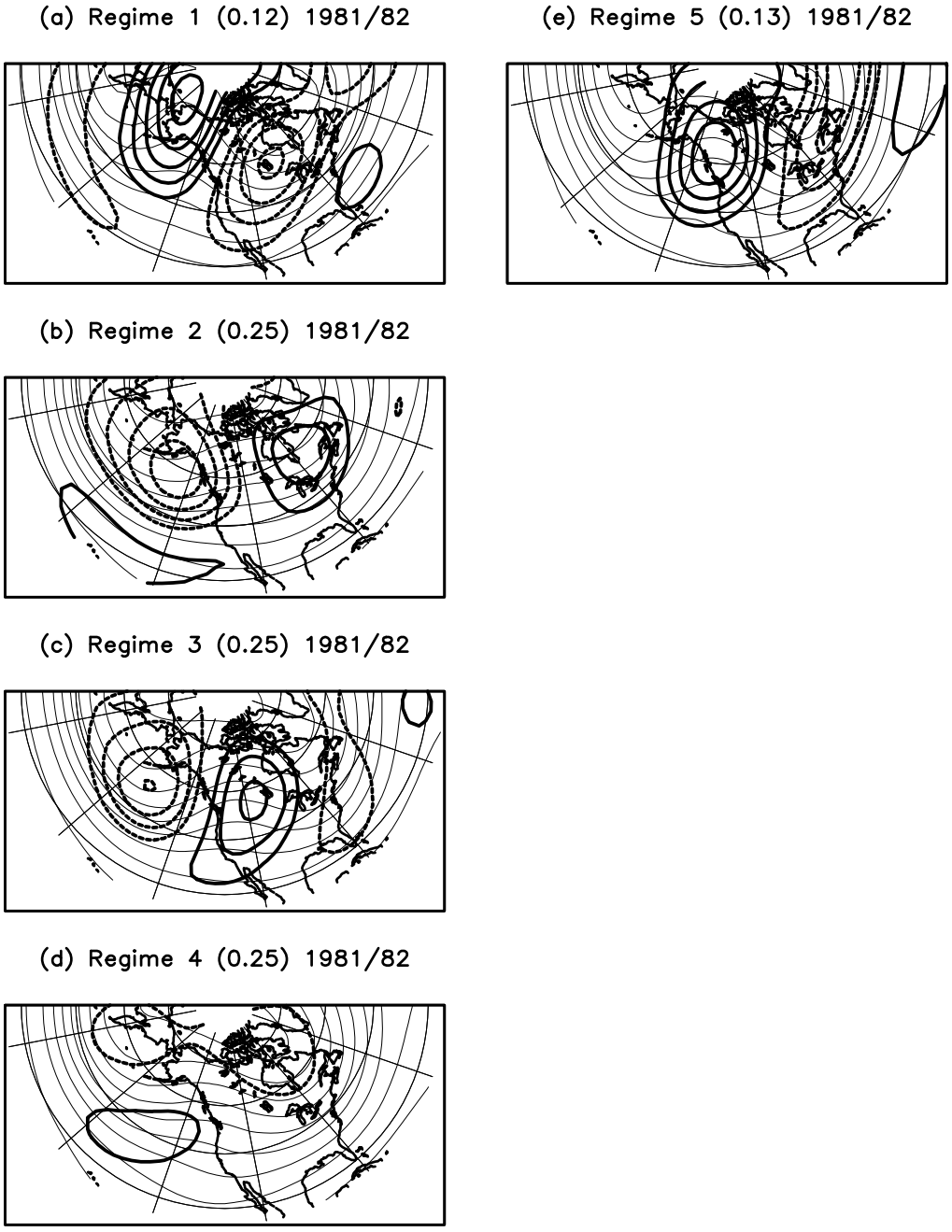

Figure 8: Average 200 hPa height for k=5 regimes. Light solid lines are total height, with a contour interval of 200 m, dark solid lines are anomalies with respect to GCM climate, with contour interval of 50 m. (Negative anomalies indicated by dark dashed lines.) (a)-(e), Regimes 1-5 for winter of 1981/82. Regimes are ordered by the area integral of the variance. The relative fraction of the regime residence is provided on the figure by the number in parenthesis (see text for explanation).

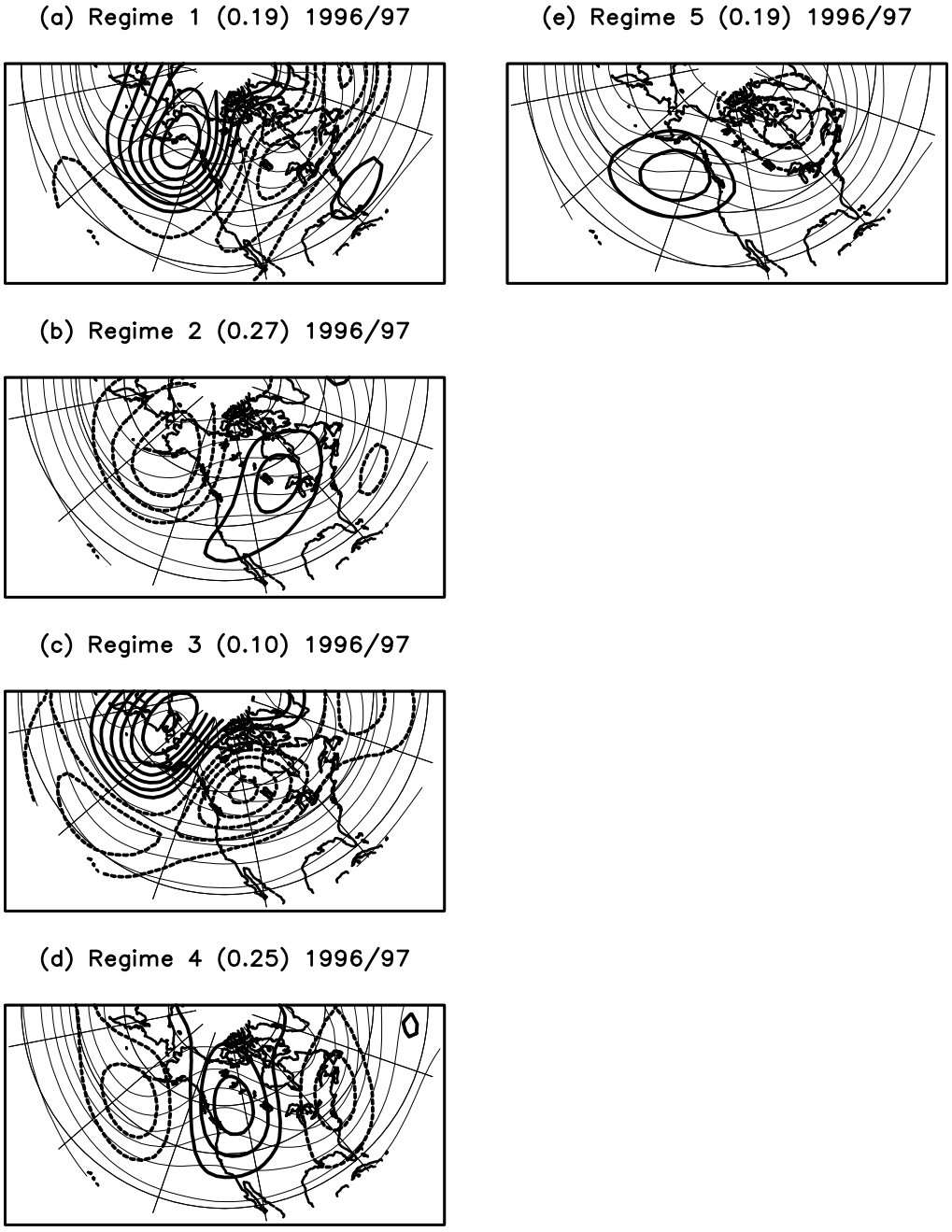

Figure 9: Average 200 hPa height for k=5 regimes. Light solid lines are total height, with a contour interval of 200 m, dark solid lines are anomalies with respect to GCM climate, with contour interval of 50 m. (Negative anomalies indicated by dark dashed lines.) (a)-(e), Regimes 1-5 for winter of 1996/97. Regimes are ordered by the area integral of the variance. The relative fraction of the regime residence is provided on the figure by the number in parenthesis (see text for explanation).

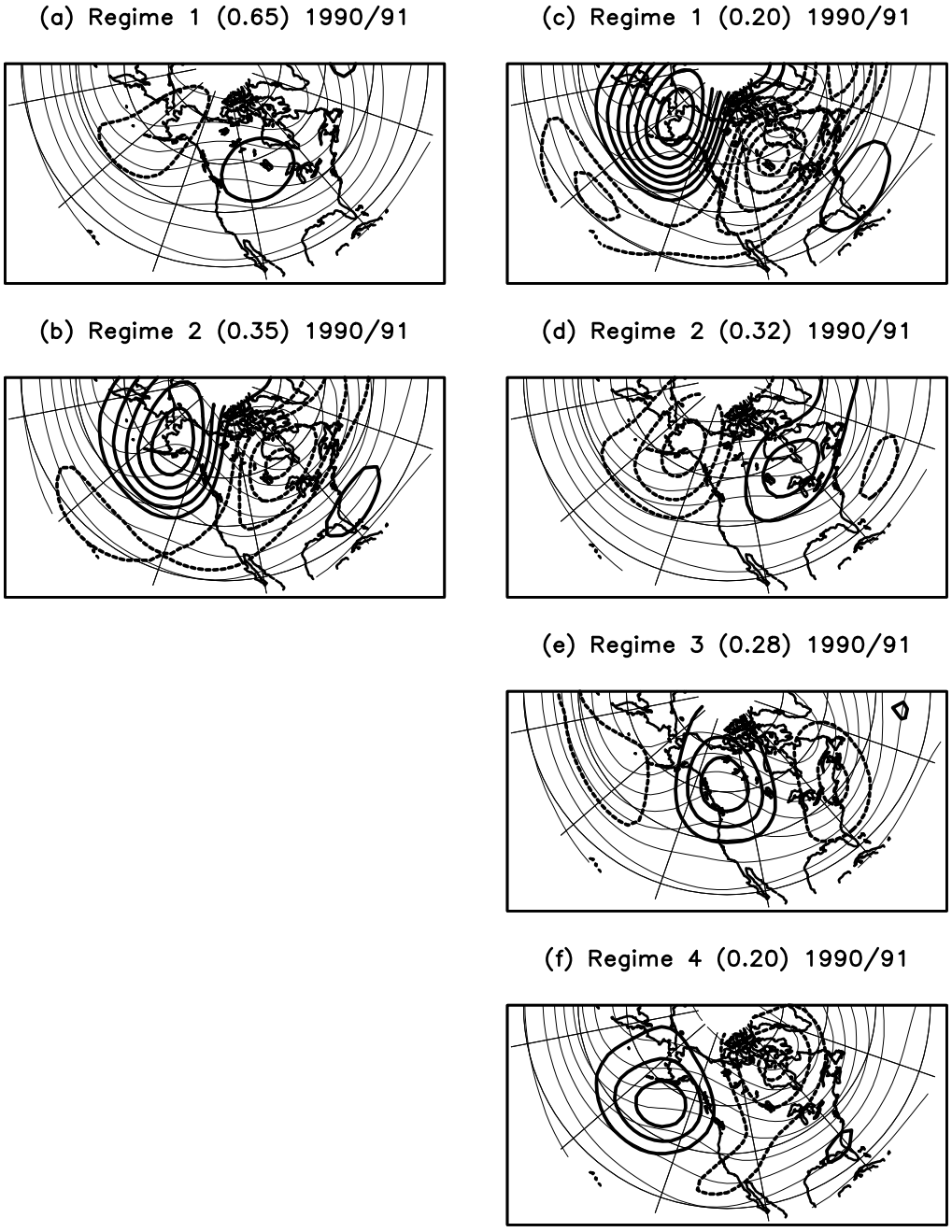

Figure 10: Average 200 hPa height for regimes for winter of 1990/91. Light solid lines are total height, with a contour interval of 200 m, dark solid lines are anomalies with respect to GCM climate, with contour interval of 50 m. (Negative anomalies indicated by dark dashed lines.) (a)-(b), Regimes 1-2 for k=2, (c)-(f), Regimes 1-4 for k=4. Regimes are ordered by the area integral of the variance. The relative fraction of the regime residence is provided on the figure by the number in parenthesis (see text for explanation).

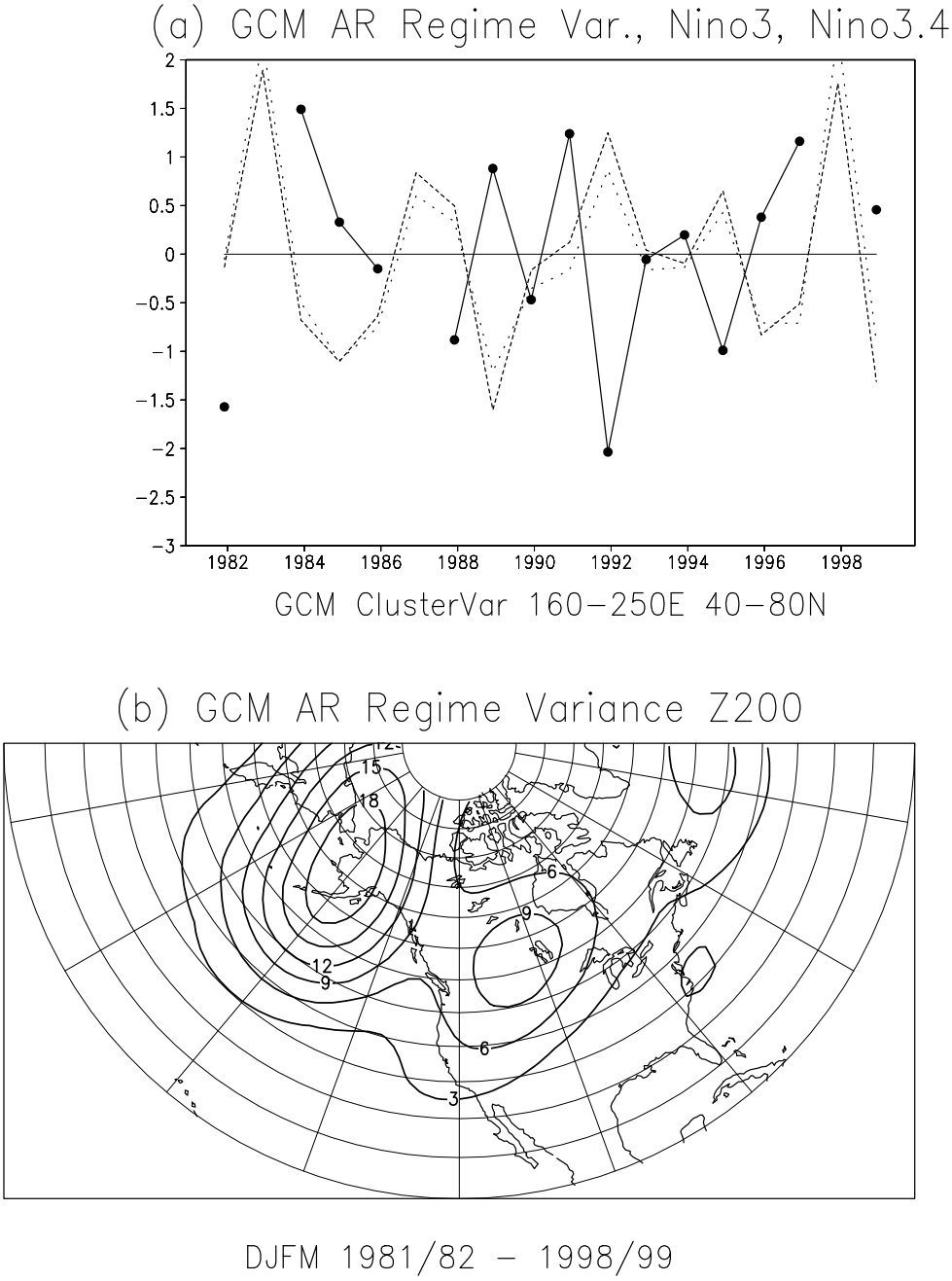

Figure 11: Variance of 200 hPa height associated with the amplified ridge (AR) regime in the GCM, obtained by summing the square of the time series over all occurrences of the AR regime, and dividing by 96 (see text for complete explanation). (a) Variance integrated over the North Pacific region $160^oE - 110^oW$, $40^oN - 80^oN$ (solid curve), Niño-3 index (dotted curve), Niño-3.4 index (dashed curve). (The indices are for the period of Dec.-Feb.) (b) Map of AR variance. Contour interval is 3000 m^2.

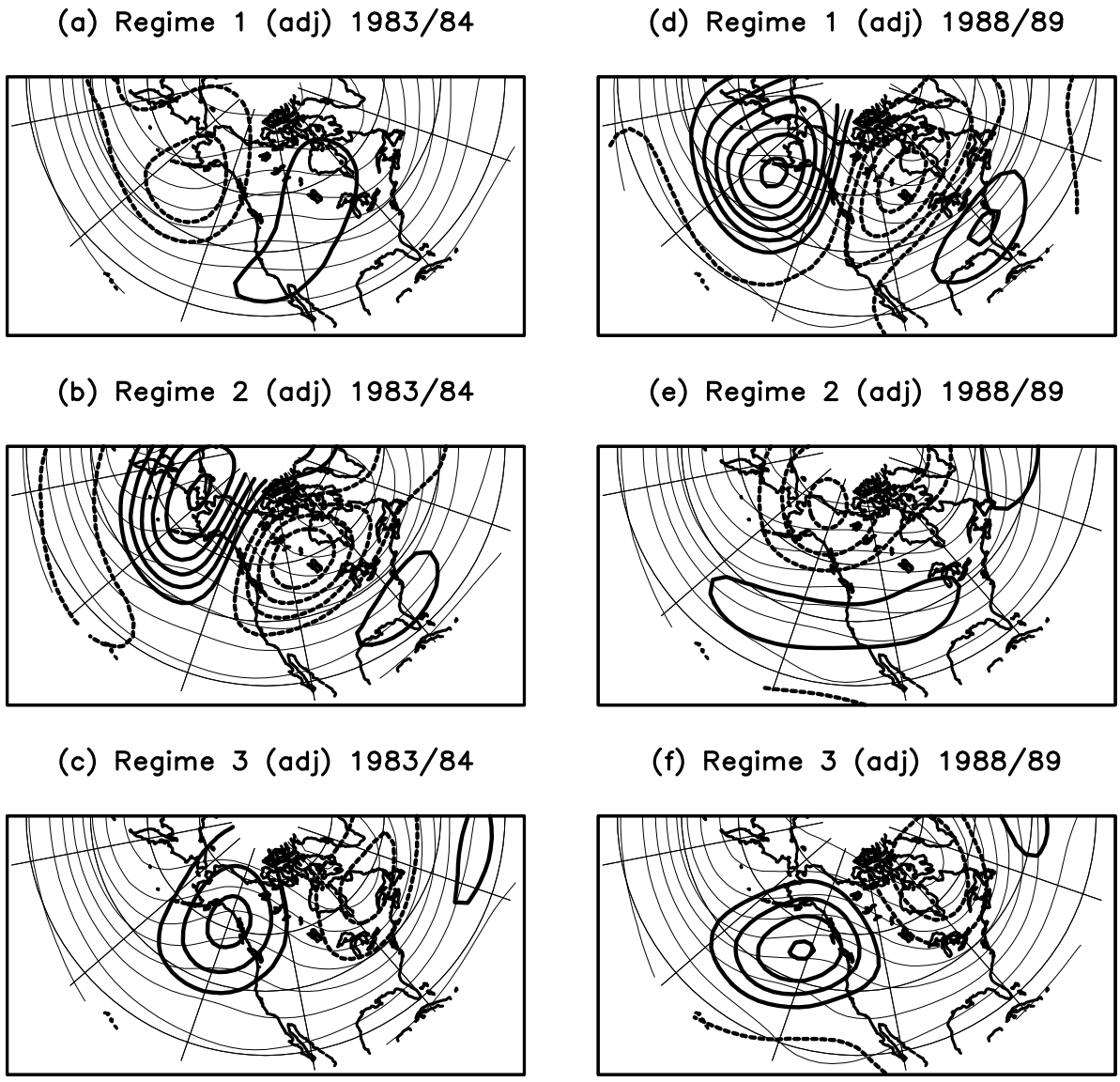

Figure 12: Average 200 hPa height for k=3 regimes when only low frequency fluctuations are included (ultra-low frequency fluctuations excluded). Light solid lines are total height, with a contour interval of 200 m, dark solid lines are anomalies with respect to GCM climate, with contour interval of 50 m. (Negative anomalies indicated by dark dashed lines.) (a)-(c), Regimes 1-3 for winter of 1983/84, (d)-(f), Regimes 1-3 for winter of 1988/89. Regimes are ordered by the area integral of the variance (see text for explanation).

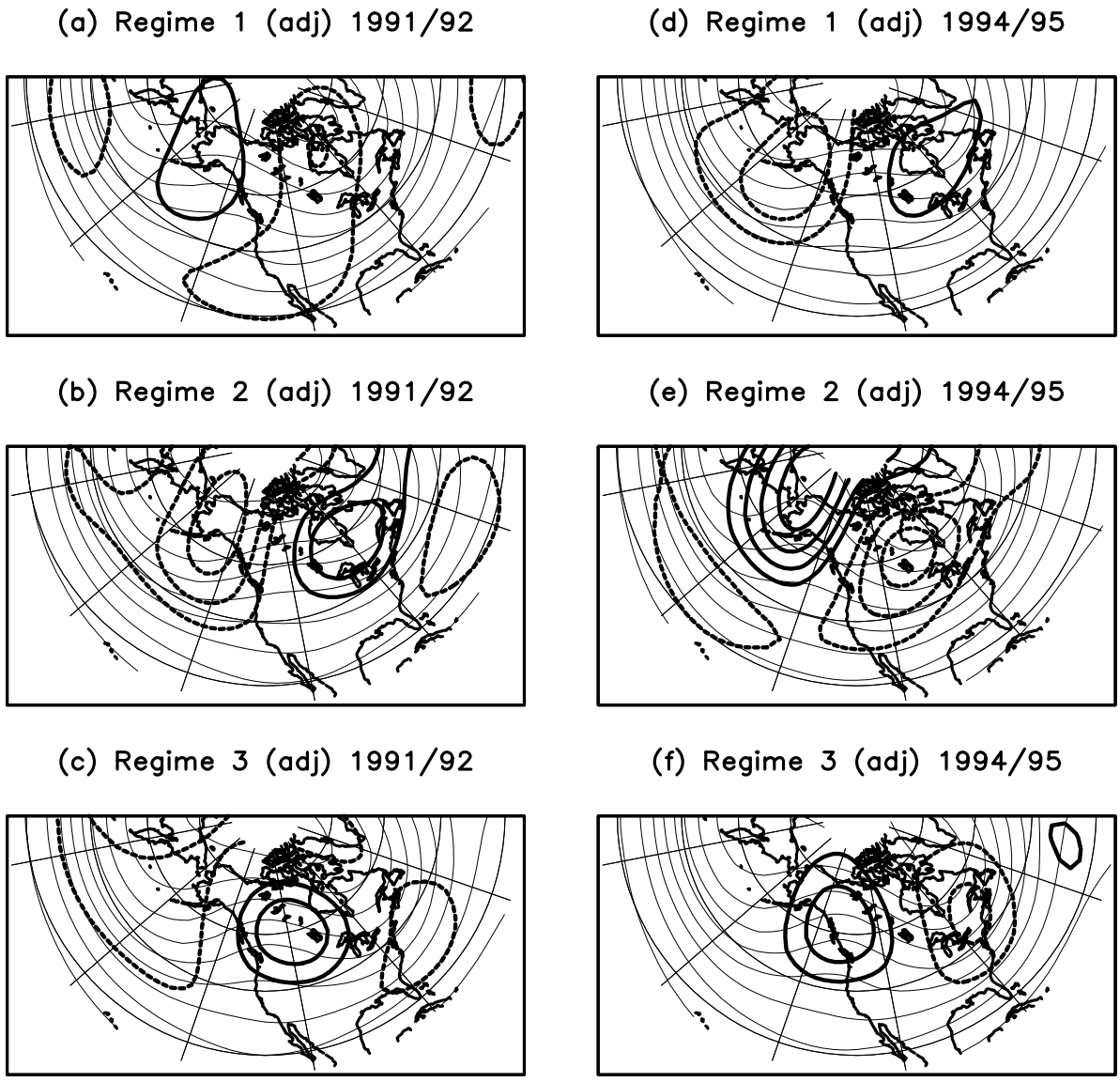

Figure 13: Average 200 hPa height for k=3 regimes when only low frequency fluctuations are included (ultra-low frequency fluctuations excluded). Light solid lines are total height, with a contour interval of 200 m, dark solid lines are anomalies with respect to GCM climate, with contour interval of 50 m. (Negative anomalies indicated by dark dashed lines.) (a)-(c), Regimes 1-3 for winter of 1991/92, (d)-(f), Regimes 1-3 for winter of 1994/95. Regimes are ordered by the area integral of the variance (see text for explanation).

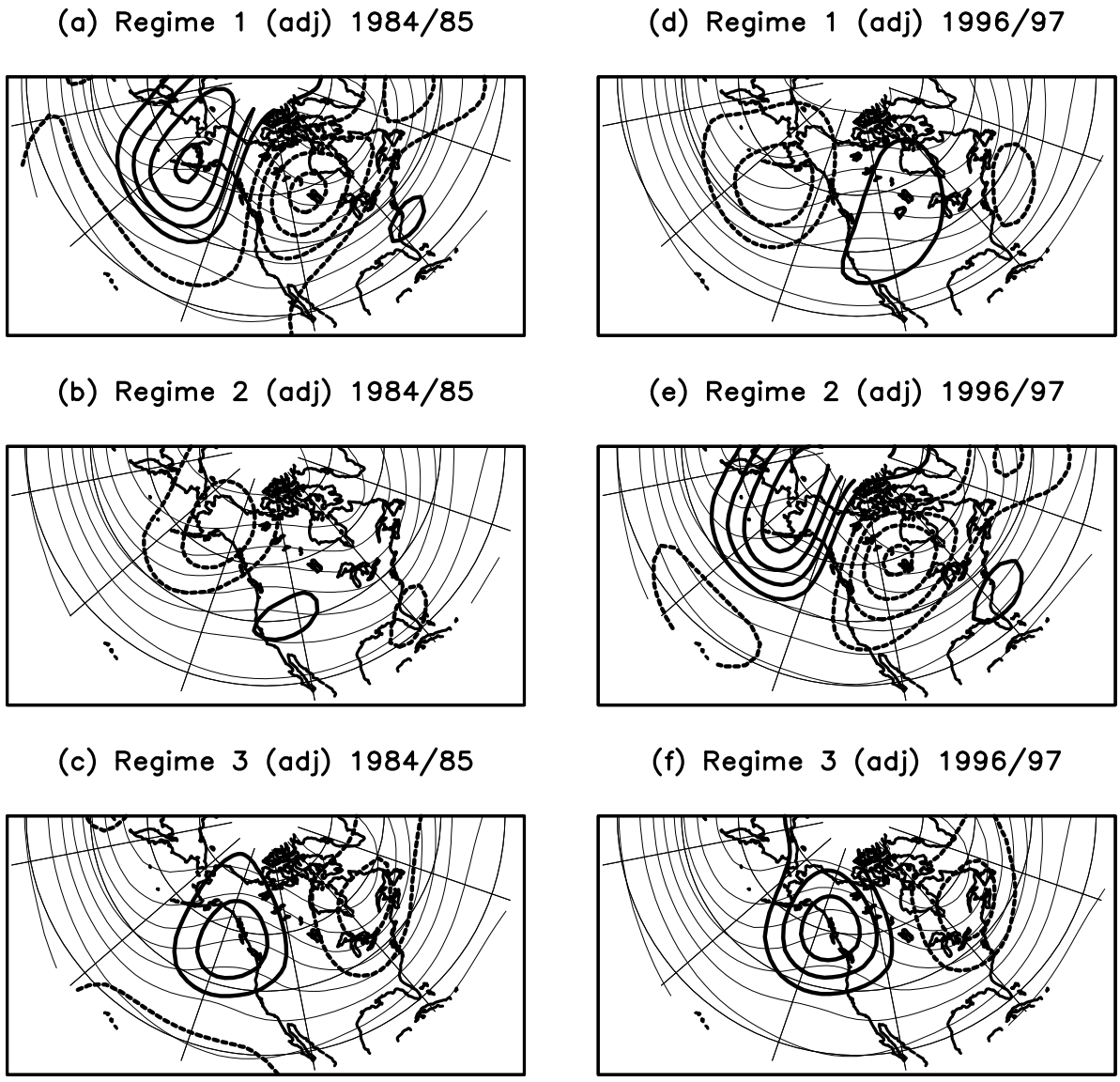

Figure 14: Average 200 hPa height for k=3 regimes when only low frequency fluctuations are included (ultra-low frequency fluctuations excluded). Light solid lines are total height, with a contour interval of 200 m, dark solid lines are anomalies with respect to GCM climate, with contour interval of 50 m. (Negative anomalies indicated by dark dashed lines.) (a)-(c), Regimes 1-3 for winter of 1984/85, (d)-(f), Regimes 1-3 for winter of 1996/97. Regimes are ordered by the area integral of the variance (see text for explanation).

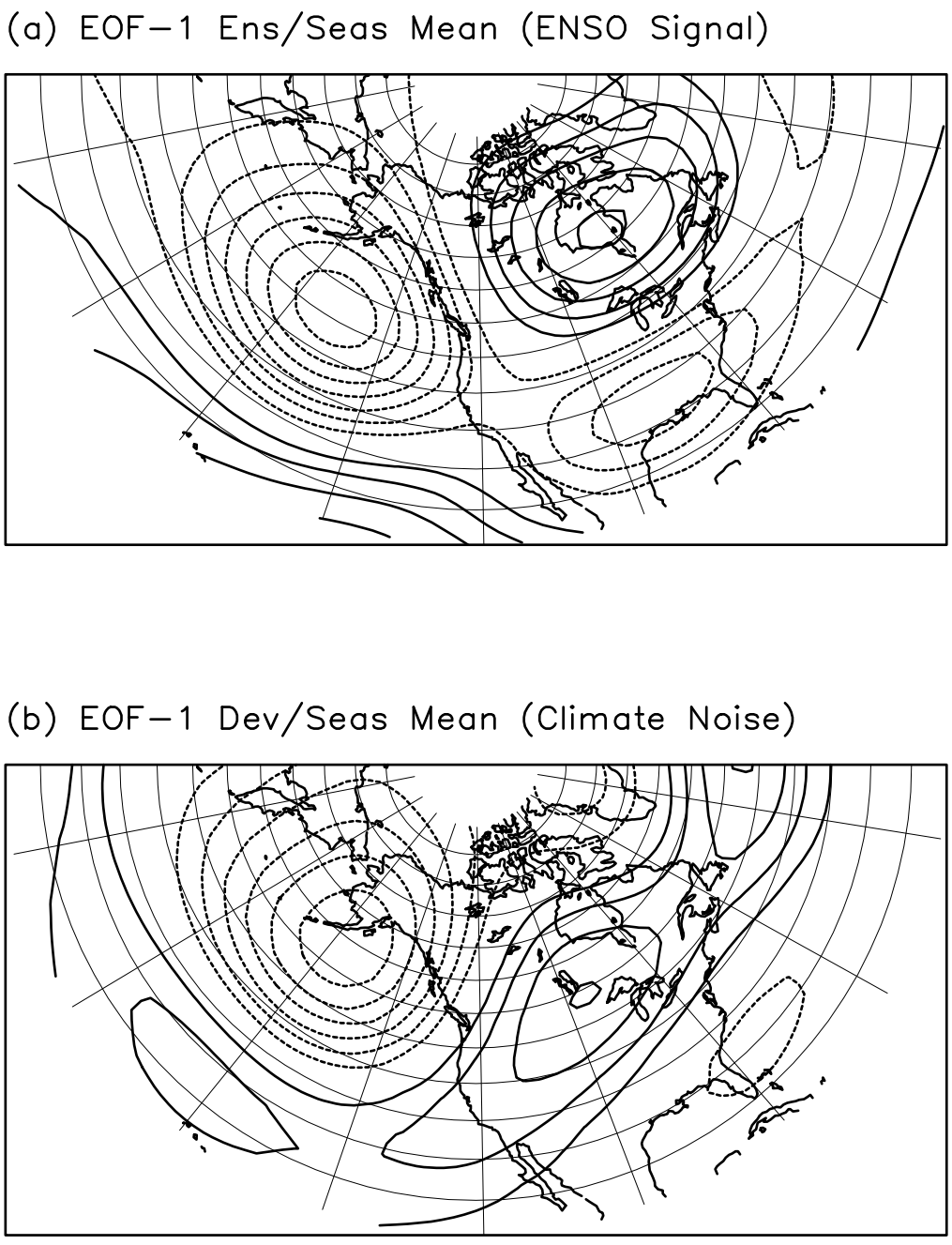

Figure 15: EOFs of SST-forced signal (a) and noise (b) in the seasonal mean. The signal is computed as the leading EOF of the 18-winter time series of the ensemble seasonal means. The noise is computed as the leading EOF of the 55×18 deviations of the seasonal mean about the ensemble mean. Contours are dimensionless.